Inorganic Chemistry, 2017, vol. 56, p. 1679-1695-1695, ISSN: 0020-1669,
doi: 10.1021/acs.inorgchem.6b02668

Circular and Chainlike Copper(II)-Lanthanide(III) Complexes Generated by Assembly Reactions of Racemic and Chiral Copper(II) Ligand-Complex with $Ln^{III}(NO_3)_3·6H_2O$ (Ln^{III} = Gd^{III}, Tb^{III}, and Dy^{III})

Takahiro Ueno,[†] Takeshi Fujinami,[†] Naohide Matsumoto,[*,†] Masaki Furusawa,[†] Ryo Irie,[†] Nazzareno Re,[§] Takuya Kanetomo,[‡] Takayuki Ishida[‡], Yukinari Sunatsuki[*,∥]

[†]Department of Chemistry, Faculty of Science, Kumamoto University, Kumamoto 860-8555, Japan

[§]Facolta di Farmacià, Universita degli Studi "G.D 'Annunzio", I-66100 Chieti, Italy

[‡]Department of Engineering Science, The University of Electro-Communications, Chofu, Tokyo 182-8585, Japan

[∥]Department of Chemistry, Faculty of Science, Okayama University, Tsushima-naka 3-1-1, Okayama 700-8530, Japan

Supporting Information

ABSTRACT: The 1:1 assembly reaction of the racemic form of the cross-linking ligand-complex $Na[Cu^{II}L^{dpen(1R2R/1S2S)}]$ with $Ln^{III}(NO_3)_3·6H_2O$ gave a centrosymmetric circular $(Cu^{II}Ln^{III})_2$ complex $[Cu^{II}L^{dpen(1R2R/1S2S)}Ln^{III}(NO_3)_2]_2$ (**1Gd**, **1Tb**, **1Dy**), while the reaction of the enantiopure form $Na[Cu^{II}L^{dpen(1R2R)}]$ with $Ln^{III}(NO_3)_3·6H_2O$ gave a chiral chainlike $(Cu^{II}Ln^{III})_{1\infty}$ complex $[Cu^{II}L^{dpen(1R2R)}Ln^{III}(NO_3)_2(CH_3CN)]_{1\infty}·CH_3CN$ (**2Gd**, **2Tb**, **2Dy**), where $\{Cu^{II}L^{dpen(1R2R)}\}^-$ is (*N*-((1*R*,2*R*)-2-(((*E*)-3-ethoxy-2-oxybenzylidene)amino)-1,2-diphenylethyl)-2-oxybenzamide)copper(II) and $\{Cu^{II}L^{dpen(1R2R/1S2S)}\}^-$ is the racemic mixture of $\{Cu^{II}L^{dpen(1R2R)}\}^-$ and $\{Cu^{II}L^{dpen(1S2S)}\}^-$. The copper(II) component functions as a cross-linking ligand-complex and bridges two Ln^{III} ions at two phenoxo oxygen atoms and one ethoxy oxygen atom, as well as at an amido oxygen atom. For **1Gd**, **1Tb**, and **1Dy**, two racemic binuclear species of $[Cu^{II}L^{dpen(1R2R)}Ln^{III}(NO_3)_2]$ and $[Cu^{II}L^{dpen(1S2S)}Ln^{III}(NO_3)_2]$ with opposite chiralities are linked by two amido oxygen atoms O3 and O3* to form a centrosymmetric circular structure with Gd−Cu = 3.370(1) Å and Gd−Cu* = 5.627(1) Å. For **2Gd**, **2Tb**, and **2Dy**, binuclear species with the same chirality are bridged by Gd−O3* = 2.228(5) Å to form a chiral chainlike structure with Gd−Cu = 3.3348(9) Å and Gd−Cu* = 6.2326(9) Å. The bridged angles through the amido group of Gd−O3*=C7* are 133.9(5)° and 177.6(4)° for **1Gd** and **2Gd**, respectively. The magnetic susceptibilities of **1Gd** and **2Gd** were analyzed by the spin-only Hamiltonian based on the circular tetranuclear $(-Cu^{II}Gd^{III}-)_2$ and linear chainlike $(-Cu^{II}Gd^{III}-)_{1\infty}$ structures, respectively. The Cu^{II}-Gd^{III} magnetic interactions through two phenoxo bridges and a three-atom N−C=O bridge, J_1 and J_2, are both positive to be $J_1 = +4.6\ cm^{-1}$ and $J_2 = +1.8\ cm^{-1}$ for **1Gd** and $J_1 = +4.2\ cm^{-1}$ and $J_2 = +0.037\ cm^{-1}$ for **2Gd**. The J_2 value of **2Gd** is much smaller than that of **1Gd**. Upon lowering the temperature, **1Ln** and **2Ln (Ln = Tb, Dy)** showed the decrease in the $\chi_M T$ vs T plot due to the crystal field effect on the Ln^{III} ion (Stark splitting) and the increase due to the ferromagnetic Cu^{II}-Ln^{III} interaction. The magnetization values of **1Ln** and **2Ln (Ln = Tb, Dy)** without liquid paraffin are considerably larger than the corresponding values with liquid paraffin, indicating the presence of strong magnetic anisotropy. **1Tb** and **1Dy** showed frequency dependence of ac magnetic susceptibility under zero external dc magnetic field, showing the behavior of single-molecule magnets (SMMs). **2Tb** and **2Dy** showed no frequency dependence under a zero external magnetic field, but showed a meaningful frequency dependence under an external magnetic field. Their energy barriers, Δ/k_B, estimated by the Arrhenius plots are 29.4(6) K and 20.6(3) K for **1Tb** and **2Tb** in the dc bias field of 0 and 1000 Oe, respectively.

INTRODUCTION

The self-assembly reaction has been applied for the formation of supramolecules and multidimensional materials.[1] Molecular-based magnets have been successfully synthesized by the assembly reaction of multicomponents, which have the donor and acceptor coordination abilities.[2-7] The donor and acceptor components have magnetic moments and the magnetic interaction between them extends to the supramolecule or dimensional lattice, depending on the nature of the magnetic interaction and the assembly manner, to produce various molecular-based magnetic materials. The representative molecular-based magnets, $MnCu(pba)(H_2O)_3·2H_2O$, $MnCu(pbaOH)(H_2O)_3$ (pba =1,3-propylenebis(oxamato), pbaOH = 2-hydroxy-1,3-propylene-bis(oxamato)),[2] $Mn(hfa)_2NIT$-R (hfa = hexafluoroacetylacetonato, and NIT-R (R = *iso*-propyl, phenyl) = 2-R-4,4,5,5-tetramethyl-4,5-dihydro-1-*H*-imidazoyl-1-oxy-3-oxide),[3] $[Fe(Me_5C_5)_2]^{·+}$ $[TCNE]^{·-}·MeCN$ ($[Fe(Me_5C_5)_2]^{·+}$ = decamethylferrocenium, $[TCNE]^{·-}$ = tetracyanoethenide),[4] $NBu_4[M^{II}Cr^{III}(ox)_3]$ (NBu_4 = tetra(*n*-butyl)ammonium, M^{II} = Mn^{2+}, Fe^{2+}, Co^{2+}, Ni^{2+}, Cu^{2+}, Zn^{2+}),[5] and $[\{Fe^{III}(CN)_6\}_n\{Mn^{III}(BS)\}_m]^{x-}$ ((n, m) = (1, 1), (1, 2), (1, 4); BS = N_2O_2 salen-type Schiff-base ligand)[6], are all synthesized by the assembly reaction of the donor and acceptor components. The assembly structure involving the donor/acceptor ratio depends on the selection of the proper components, in which the stereochemistry and the electronic effects by modifications of the ligand and metal ions can result in different assembly structures. There are many cases in which the steric effect from the substituent of the ligand produces different assembly structures.[2-7] For example, (1) the *iso*-propyl and phenyl substituents of $Mn(hfa)_2NIT$-R give 1D and cyclic hexanuclear structures,[3] respectively, and (2) the methyl and the phenyl substituents in $[Cu^{II}L^R]$ (L^R = *N*-(2-R-imidazol-4-ylmethylidene)-2-aminoethylpyridine, R = methyl and phenyl) give cyclic tetranuclear and hexanuclear structures, respectively.[8] The chirality must be a relevant element to generate the definitely different assembly structure, as exemplified by spontaneous resolution of tartaric acid salts.[9] However, there are only a few examples in which the chirality of the component produces different assembly structures in the molecular-based magnet.[10] In addition to the assembly structure, the chirality in the molecular-based magnets has attracted much attention recently in evolving new functions, like nonlinear magnetic property and chiral magnetic effects.[11, 12]

In this study, we report that chiral discriminative assembly reactions of racemic and chiral Cu^{II} complexes with $Ln^{III}(NO_3)_3·6H_2O$ produce distinctly different structures: centrosymmetric circular $(Cu^{II}Ln^{III})_2$ and chiral 1D $(Cu^{II}Ln^{III})_{1\infty}$ structures. As shown in Scheme 1, the chiral and racemic Cu^{II} complexes used in this study are of $Na[Cu^{II}L^{dpen(1R2R)}]$ and $Na[Cu^{II}L^{dpen(1S2S)}]$, and $Na[Cu^{II}L^{dpen(1R2R/1S2S)}]$, respectively, where $H_3L^{dpen(1R2R)}$ is a chiral N_2O_2 ligand abbreviated from *N*-((1*R*,2*R*)-2-(((*E*)-3-ethoxy-2-hydroxybenzylidene)-amino)-1,2-diphenylethyl)-2-hydroxybenzamide, $H_3L^{dpen(1R2R)}$ denotes its *1S*,*2S* form, and $H_3L^{dpen(1R2R/1S2S)}$ is the racemic ligand. The Cu^{II} complex acts as a cross-linking ligand-complex with donor coordination abilities to Ln^{III} ion at two phenoxo oxygen atoms and one ethoxy oxygen atom of one side of the square planar complex and at an amido oxygen atom on the other side. $Ln^{III}(NO_3)_3·6H_2O$ functions as an acceptor component, exhibiting acceptor coordination abilities at both the vacant and substitutable coordination sites. As shown in Scheme 1, the assembly reaction of the racemic Cu^{II} component $Na[Cu^{II}L^{dpen(1R2R/1S2S)}]$ with $Ln^{III}(NO_3)_3·6H_2O$ gave a centrosymmetric circular $(Cu^{II}Ln^{III})_2$ complex $[Cu^{II}L^{dpen(1R2R/1S2S)}\text{-}Ln^{III}(NO_3)_2]_2$·solvent (**1Gd**, **1Tb**, **1Dy**). On the other hand, the reaction of the chiral Cu^{II} component $Na[Cu^{II}L^{dpen(1R2R)}]$ with $Ln^{III}(NO_3)_3·$ $6H_2O$ gave a chiral chainlike $(Cu^{II}Ln^{III})_{1\infty}$ complex $[Cu^{II}L^{dpen(1R2R)}Ln^{III}(NO_3)_2(CH_3CN)]_{1\infty}·CH_3CN$ (**2Gd**, **2Tb**, **2Dy**).

The Cu^{II} component has a magnetic moment due to $S = 1/2$ spin state of its d^9 electronic configuration. The Ln^{III} ions used in this study are Gd^{III}, Tb^{III}, and Dy^{III}, and they have large magnetic moments due to their ground states: Gd^{III} ($4f^7$, $J = 7/2$, $S = 7/2$, $L = 0$, $^8S_{7/2}$), Tb^{III} ($4f^8$, $J = 6$, $S = 3$, $L = 3$, $^7F_6$), and Dy^{III} ($4f^9$, $J = 15/2$, $S = 5/2$, $L = 5$, $^6H_{15/2}$).[13] Magnetic interaction can occur between Cu^{II} and Ln^{III} ions through phenoxo and amido groups. For $Cu^{II}Ln^{III}$ complexes ($Ln^{III} = Gd^{III}$, Tb^{III}, Dy^{III}), it has been known that ferromagnetic interaction through various bridging groups is operating.[14] Therefore, it is anticipated that the magnetic interaction in the supramolecule or crystal lattice, depending on the assembly structure to give molecular-based magnets. While the Gd^{III} ion is magnetically isotropic due to the ground state of Gd^{III} ($4f^7$, $J = 7/2$, $S = 7/2$, $L = 0$, $^8S_{7/2}$), the Tb^{III} and Dy^{III} ions have large magnetic anisotropy due to the ground states of Tb^{III} ($4f^8$, $J = 6$, $S = 3$, $L = 3$, $^7F_6$) and Dy^{III} ($4f^9$, $J = 15/2$, $S = 5/2$, $L = 5$, $^6H_{15/2}$). Since the discovery of single-molecule magnets (SMMs) in a Mn_{12} cluster in 1993,[15] many synthetic designs for SMMs have been developed based on d-cluster molecules,[16] mononuclear and polynuclear f-complexes,[17] and d−f complexes.[18] A high-spin ground state and large magnetic anisotropy are required for the synthetic design of SMMs. Thus, it is anticipated that Cu^{II}-Ln^{III} complexes with $Ln^{III} = Tb^{III}$ and Dy^{III} would exhibit SMM behaviors. Two pairs of Cu^{II}-Ln^{III} complexes with circular and chainlike structures, (**1Tb**, **2Tb**) and (**1Dy**, **2Dy**), would be good candidates for SMM and single-chain magnet (SCM).[19] We report here the synthesis, structures, and magnetic properties of these complexes.

Scheme 1. Chiral discriminative assembly reactions of the racemic and chiral Cu^{II} components of $[Cu^{II}L^{dpen(1R2R/1S2S)}]^-$ and $[Cu^{II}L^{dpen(1R2R)}]^-$ with $Gd^{III}(NO_3)_3·6H_2O$, leading to centrosymmetric circular 1Gd and chiral chainlike 2Gd structures

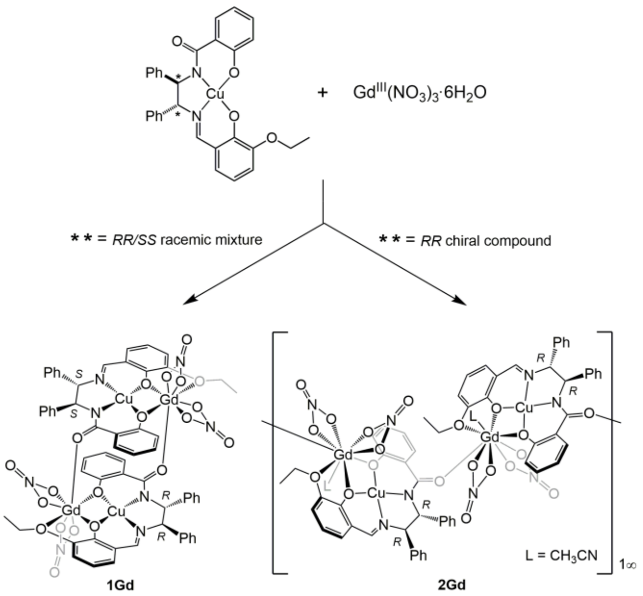

RESULTS AND DISCUSSION

Synthesis and Characterization of Circular and Chainlike Cu^{II}-Ln^{III} Complexes ($Ln^{III} = Gd^{III}$, Tb^{III}, Dy^{III}) $[Cu^{II}L^{dpen(1R2R/1S2S)}Ln^{III}(NO_3)_2(H_2O)]_2$ (1Gd, 1Tb, 1Dy) and $[Cu^{II}L^{dpen(1R2R)}$ $Ln^{III}(NO_3)_2(H_2O)]_{1\infty}$ (2Gd, 2Tb, 2Dy). Racemic and optically pure N_2O_2 ligands, $H_3L^{dpen(1R2R/1S2S)}$, $H_3L^{dpen(1R2R)}$**,** and $H_3L^{dpen(1S2S)}$, were prepared by a two-step reaction via intermediate compounds. In the first step of the synthesis of the racemic ligand $H_3L^{dpen(1R2R/1S2S)}$, the 1:1 condensation product of phenylsalicylate and a racemic mixture of (1*R*,2*R*/1*S*,2*S*)-1,2-diphenylethanediamine, i.e., *N*-((1*R*,2*R*/1*S*,2*S*)-2-amino-1,2- diphenylethyl)-2-hydroxybenzamide, was obtained as an intermediate compound. The 1:1 product was reacted with 3-ethoxysalicylaldehyde in a 1:1 molar ratio to give the tetradentate ligand $H_3L^{dpen(1R2R/1S2S)}$ as a yellow crystalline material. The chiral tetradentate ligands $H_3L^{dpen(1R2R)}$ and $H_3L^{dpen(1S2S)}$ are similarly synthesized using (1*R*,2*R*)-1,2-diphenylethylenediamine and (1*S*,2*S*)-1,2-diphenylethylenediamine, respectively.

The racemic Cu^{II} complex $Na[Cu^{II}L^{dpen(1R2R/1S2S)}]$·solvent was synthesized by mixing the racemic ligand $H_3L^{dpen(1R2R/1S2S)}$, copper(II) acetate monohydrate, and NaOH in a 1:1:3 molar ratio in methanol. The resulting crude product was recrystallized from a mixed solution of acetonitrile and a small amount of ethanol to precipitate deep-red block crystals with the formula $Na[Cu^{II}L^{dpen(1R2R/1S2S)}]·CH_3CN$, as confirmed by X-ray structural analysis. The crystals exhibited efflorescence to eliminate the acetonitrile molecule and partially absorb the moisture under the open atmosphere, giving the product with the chemical formula $Na[Cu^{II}L^{dpen(1R2R/1S2S)}]·H_2O·0.5CH_3CN$. The elemental analysis agrees with the formula and the detailed efflorescence process was confirmed by TGA analysis (Supplementary Material S1). TGA analysis detected weight loss corresponding to $H_2O·0.5CH_3CN$, and this result agrees with the elemental analysis. The optically pure complex $Na[Cu^{II}L^{dpen(1R2R)}]$·solvent was synthesized by mixing the optically pure $H_3L^{dpen(1R2R)}$, copper(II) acetate monohydrate, and NaOH in a 1:1:3 molar ratio in methanol. The resulting crude product was recrystallized from a mixed solution of acetonitrile and a small amount of ethanol to obtain deep-red block crystals with the formula $Na[Cu^{II}L^{dpen(1R2R)}]·2CH_3CN$, which was confirmed by X-ray structural analysis. The crystals exhibited efflorescence to eliminate the acetonitrile molecule and absorb the moisture under open atmosphere, giving the product with the chemical formula $Na[Cu^{II}L^{dpen(1R2R)}]\cdot H_2O$, which agrees with the elemental analysis. The detailed efflorescence process was confirmed by TGA analysis (Supplementary Material S1). TGA analysis detected weight loss corresponding to H_2O.

Two groups of Cu^{II}-Ln^{III} assembly complexes (Ln^{III} = Gd^{III}, Tb^{III}, Dy^{III}), $[Cu^{II}L^{dpen(1R2R/1S2S)}Ln^{III}(NO_3)_2]_2$ (**1Ln**) and $[Cu^{II}L^{dpen(1R2R)}Ln^{III}(NO_3)_2(CH_3CN)]_{1\infty}\cdot CH_3CN$ (**2Ln**), were synthesized by the assembly reaction of the racemic and optically pure Cu^{II} components $Na[Cu^{II}L^{dpen(1R2R)}]\cdot H_2O$ and $Na[Cu^{II}L^{dpen(1R2R/1S2S)}]\cdot H_2O\cdot 0.5CH_3CN$ with Ln^{III} components $Ln^{III}(NO_3)_3\cdot 6H_2O$. In the assembly reaction, the copper(II) component functions as a cross-linking ligand-complex at the phenoxo and amide oxygen atoms. The 1:1 assembly reaction of $Na[Cu^{II}L^{dpen(1R2R/1S2S)}]\cdot H_2O\cdot 0.5CH_3CN$ and $Ln^{III}(NO_3)_3\cdot 6H_2O$ in CH_3CN gave dark gray crystals for **1Gd** and blue-green crystals for both **1Tb** and **1Dy**, with the formula $[Cu^{II}L^{dpen(1R2R/1S2S)}Ln^{III}(NO_3)_2]_2\cdot xH_2O\cdot yCH_3CN$ (x = 0 and y = 0 for **1Gd**, x = 2 and y = 2 for **1Tb**, and x = 0 and y = 2 for **1Dy**). These chemical formulas were confirmed by X-ray structural analysis. TGA analysis detected weight loss corresponding to $xH_2O\cdot yCH_3CN$. These results are given in Supplementary Material S2. The 1:1 assembly reaction of $Na[Cu^{II}L^{dpen(1R2R)}]\cdot H_2O$ and $Ln^{III}(NO_3)_3\cdot 6H_2O$ in CH_3CN gave pale red rectangular crystals of $[Cu^{II}L^{dpen(1R2R)}Ln^{III}(NO_3)_2(CH_3CN)]_{1\infty}\cdot CH_3CN$ (**2Ln**). The crystals exhibited efflorescence to eliminate the acetonitrile molecule and absorb the atmospheric moisture under open atmosphere, giving the product with the chemical formula $[Cu^{II}L^{dpen(1R2R)}Ln^{III}(NO_3)_2]_{1\infty}\cdot 1.5H_2O$. The detailed efflorescence process was confirmed by TGA analysis (Supplementary Material S3). TGA analysis detected weight loss corresponding to $1.5H_2O$ and these results agree with the elemental analysis.

The IR spectra of the ligands, Cu^{II} complexes, and Cu^{II}-Ln^{III} complexes showed the characteristic strong peaks assignable to C=N and C=O stretching vibrations. The C=N stretching vibrations for the ligands, Cu^{II} complexes, **1Ln**, and **2Ln** were observed at 1626, 1625−1624, 1634, and 1634−1633 cm^{-1}, respectively. The amido C=O stretching vibrations of the ligands, Cu^{II} complexes, **1Ln**, and **2Ln** were observed at 1595−1589, 1567−1561, 1576−1574, and 1570 cm^{-1}, respectively.[18c] The amido C=O peak is affected by the coordination to the Ln^{III} ion and the bridging mode. The bridging angle of the C=O−Ln of **2Ln** is larger than that of **1Ln**, as described in the X-ray section.

STRUCTURAL DESCRIPTION

Racemic Copper(II) Complex $[(CH_3CN)NaCu^{II}$-$L^{dpen(1R2R/1S2S)}]$. Table 1 shows the X-ray crystallographic data for the racemic and chiral copper(II) component complexes. Table 2 shows their relevant bond distances and angles. The racemic copper(II) complex $[(CH_3CN)NaCu^{II}$-$L^{dpen(1R2R/1S2S)}]$ crystallized into a centrosymmetric space group *P*bca (No. 61). The crystallographically unique unit consists of one Na^+ cation, one complex-anion $[Cu^{II}L^{dpen(1R2R)}]^-$ or mirror imaged $[Cu^{II}L^{dpen(1S2S)}]^-$, and one CH_3CN molecule. Figure 1 shows the molecular structures of $[(CH_3CN)NaCuL^{dpen(1R,2R)}]$ with the selected atom numbering scheme. The Cu^{II} ion has a square-planar coordination geometry with N_2O_2 donor atoms of a trinegative tetradentate ligand $(L^{dpen(1R2R)})^{3-}$. The coordination bond distances are Cu−O(1) = 1.881(3), Cu−O(2) = 1.907(3), Cu−N(1) = 1.889(4), and Cu−N(2) = 1.922(4) Å, in which the Cu−O(2) and Cu−N(2) bond distances at the 3-ethoxysalicylaldehyde moiety are longer than the corresponding values of Cu−O(1) and Cu−N(1) at the 2-oxybenzamido moiety. This demonstrates that the NO donors of the 2-oxy-3-ethoxybenzylidene moiety give a weaker ligand field than those of the 2-oxybenzamido moiety.

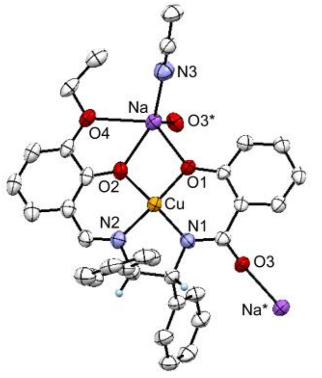

Figure 1. Molecular structure of $[(CH_3CN)NaCuL^{dpen(1R2R/1S2S)}]$ with the selected atom numbering scheme. Hydrogen atoms except for those of the (1*R*,2*R*)-diphenylethane moiety are omitted for clarity.

The Na^+ ion is coordinated by four oxygen atoms—two phenoxo oxygen atoms, O(1) and O(2), and one ethoxy oxygen atom O(4), along with an amido oxygen atom, O(3)*, of an adjacent anion-complex $[Cu^{II}L^{dpen(1R2R)}]^-$ (*; 1−x, 1/2+y, 1/2−z), and one nitrogen atom N(3) of CH_3CN molecule. These distances are Na−O(1) = 2.354(4), Na−O(2) = 2.274(4), Na−O(4) = 2.552(4), Na−O(3)* = 2.187(4), and Na−N(3) = 2.418(5) Å. Among the four Na−O distances, the distance of Na−O(3)* = 2.187(4) Å between a Na^+ ion and the amido oxygen atom O(3)* is the shortest. Because of the Na−O(3)* bond, the Cu^{II} complex forms a 1D chain structure as shown in Figure 2. Within a zigzag chain, the two adjacent molecules linked by a Na^+ ion are related by a symmetry operation of the 2_1-screw axis to a form homochiral 1D chain $[(CH_3CN)NaCuL^{dpen(1R,2R)}]_{1\infty}$. The adjacent chains with the different chiralities, i.e., $[(CH_3CN)NaCuL^{dpen(1R,2R)}]_{1\infty}$ and $[(CH_3CN)NaCuL^{dpen(1S,2S)}]_{1\infty}$, are arrayed along the *b*-axis to give a racemic crystal.

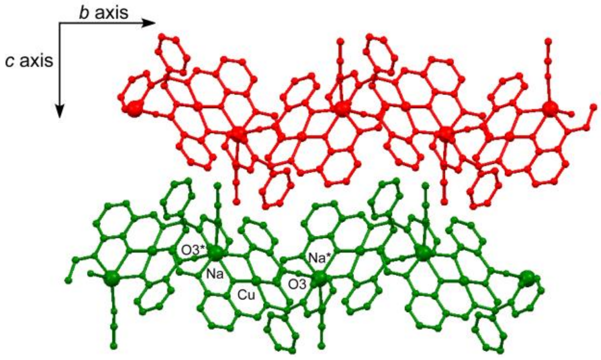

Figure 2. Adjacent 1D chains of $[(CH_3CN)NaCuL^{dpen(1R2R/1S2S)}]$. Homochiral chains with different chiralities, i.e., $[(CH_3CN)NaCuL^{dpen(1R2R)}]_{1\infty}$ (green) and $[(CH_3CN)NaCuL^{dpen(1S2S)}]_{1\infty}$ (red), run along the *b*-axis. Na^+ ion acts as a connector to form a homochiral chain.

Chiral Copper(II) Complex $[(CH_3CN)NaCu^{II}L^{dpen(1R2R)}]\cdot CH_3CN$. The chiral copper(II) complex $[(CH_3CN)NaCu^{II}L^{dpen(1R2R)}]\cdot CH_3CN$ crystallized into a chiral space group $P2_12_12_1$ (No. 19). The crystallographically unique unit consists of one Na^+ cation, one complex-anion $[Cu^{II}L^{dpen(1R2R)}]^-$, and two CH_3CN molecules. Figure 3 shows the molecular structure of $[(CH_3CN)NaCuL^{dpen(1R,2R)}]$ with the selected atom numbering scheme. The Cu^{II} ion has a square-planar coordination geometry with N_2O_2 donor atoms of a trinegative tetradentate ligand $(\mathrm{L}^{\mathrm{dpen(1R2R)}})^{3-}$. The coordination bond distances are Cu−O(1) = 1.8873(16), Cu−O(2) = 1.9157(13), Cu−N(1) = 1.9034(15), and Cu−N(2) = 1.9383(18) Å, in which the Cu−O(2) and Cu−N(2) bond distances at the 3-ethoxysalicylaldehyde moiety are longer than the corresponding values of Cu−O(1) and Cu−N(1) at the 2-oxybenzamido moiety. This demonstrates that the NO donors of the 2-oxy-3-ethoxybenzylidene moiety give a weaker ligand field than those of the 2-oxybenzamido moiety.

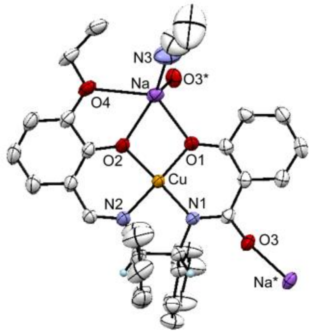

Figure 3. Structure of $[(\mathrm{CH_3CN})\mathrm{NaCuL}^{\mathrm{dpen(1R2R)}}]\cdot\mathrm{CH_3CN}$ with the selected atom numbering scheme. Hydrogen atoms except for those of the (1*R*,2*R*)-diphenylethane moiety are omitted for clarity.

Table 1. X-ray Crystallographic Data for $\mathrm{Na[Cu^{II}L^{dpen(1R2R/1S2S)}]\cdot CH_3CN}$ and $\mathrm{Na[Cu^{II}L^{dpen(1R2R)}]\cdot 2CH_3CN}$

	$\mathrm{Na[Cu^{II}L^{dpen(1R2R/1S2S)}]}$ $\mathrm{\cdot CH_3CN}$	$\mathrm{Na[Cu^{II}L^{dpen(1R2R)}]\cdot 2}$ $\mathrm{CH_3CN}$
formula	$\mathrm{C_{32}H_{28}N_3O_4CuNa}$	$\mathrm{C_{34}H_{31}N_4O_4CuNa}$
fw	605.13	646.18
cryst syst	orthorhombic	orthorhombic
space group	*Pbca* (No.61)	$P2_12_12_1$ (No.19)
a, Å	17.2573(7)	10.5113(3)
b, Å	13.7983(5)	14.3575(4)
c, Å	23.6297(8)	21.2636(6)
V, Å^3	5626.8(4)	3209.0(2)
Z	8	4
T, K	150	150
F(000)	2504.00	1340.00
$D_{\mathrm{calcd.}}$, g cm^{-3}	1.429	1.337
μ, mm^{-1}	0.8346	0.7372
λ, Å	0.71075	0.71075
R, *R*w	0.0559, 0.0892	0.0325, 0.0466
Flack	−	0.000(8)

The $\mathrm{Na^+}$ ion is coordinated by four oxygen atoms consisting of two phenoxo oxygen atoms O(1), O(2) and one ethoxy oxygen atom O(4), along with an amido oxygen atom O(3)* of an adjacent anion-complex $[\mathrm{Cu^{II}L^{dpen(1R2R)}}]^-$ (*; 1−x, 1/2+y, 1/2−z), and one nitrogen atom N(3) of $\mathrm{CH_3CN}$ molecule. These distances are Na−O(1) = 2.3326(15), Na−O(2) = 2.2891(16), Na−O(4) = 2.5691(17), Na−O(3)* = 2.1791(16), and Na−N(3) = 2.394(3) Å. Among the four Na−O distances, the distance of Na−O(3)* = 2.1791(16) Å between a $\mathrm{Na^+}$ ion and the amido oxygen atom O(3)* is the shortest. Becuase of the Na−O(3)* bond, the $\mathrm{Cu^{II}}$ complex forms a 1D chain structure running along the *b*-axis as shown in Figure 4. Within a chain, the two adjacent molecules linked by a $\mathrm{Na^+}$ ion are related by a symmetry operation of the 2_1-screw axis to form chiral 1D chain $[(\mathrm{CH_3CN})\mathrm{NaCuL}^{\mathrm{dpen(1R,2R)}}]_{1\infty}$. The adjacent chains with the same chirality are arrayed and stacked along the *b*-axis to give a chiral crystal.

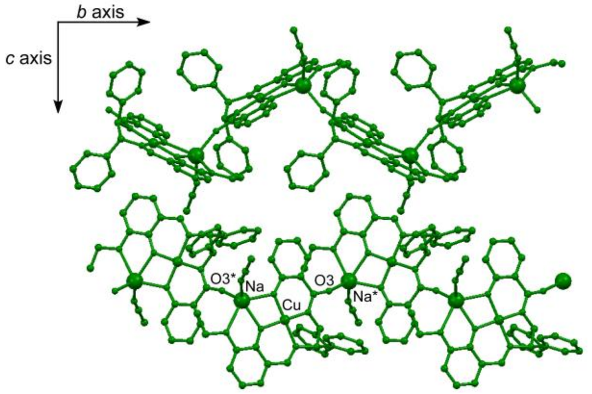

Figure 4. Adjacent 1D chains of $[(\mathrm{CH_3CN})\mathrm{NaCuL}^{\mathrm{dpen(1R2R)}}]_{1\infty}$ with same chirality running along the *b*-axis.

Table 2. Selected Coordination Bond Lengths (Å) and Angles (°) for $\mathrm{Na[Cu^{II}L^{dpen(1R2R/1S2S)}]\cdot CH_3CN}$ and $\mathrm{Na[Cu^{II}L^{dpen(1R2R)}]\cdot 2CH_3CN}$

	$\mathrm{Na[Cu^{II}L^{dpen(1R2R/1S2S)}]}$ $\mathrm{\cdot CH_3CN}$	$\mathrm{Na[Cu^{II}L^{dpen(1R2R)}]}$ $\mathrm{\cdot 2CH_3CN}$
	Bond Lengths (Å)	
Cu1−O1	1.881(3)	1.8873(16)
Cu1−O2	1.907(3)	1.9157(13)
Cu1−N1	1.889(4)	1.9034(15)
Cu1−N2	1.922(4)	1.9383(18)
Na1−O1	2.354(4)	2.3326(15)
Na1−O2	2.274(4)	2.2891(16)
Na1−O3*	2.187(4)	2.1791(16)
Na1−O4	2.552(4)	2.5691(17)
Na1−N3	2.418(5)	2.394(3)
Na1−N3	2.418(5)	2.394(3)
	Bond Angles (°)	
O1−Cu1−O2	85.96(12)	85.97(6)
O1−Cu1−N1	96.44(14)	96.29(7)
O1−Cu1−N2	175.09(14)	176.52(8)
O2−Cu1−N1	172.66(14)	176.13(7)
O2−Cu1−N2	92.42(14)	92.28(7)
O1−Na1−O2	67.80(11)	68.25(6)
O1−Na1−O3*	100.31(12)	104.10(6)
O1−Na1−N3	103.28(14)	102.55(9)
O2−Na1−O4	64.49(11)	63.29(5)
O3*−Na1−N3	120.41(15)	114.90(10)
Na1−O3*−C7*	166.3(3)	162.22(14)

(*; 1 − x, 1/2 + y, 1/2 − z)

As described above, the racemic $\mathrm{Cu^{II}}$ complex, $[(\mathrm{CH_3CN})\mathrm{NaCuL}^{\mathrm{dpen(1R2R/1S2S)}}]$, has a similar chainlike structure to the chiral $\mathrm{Cu^{II}}$ complex, $[(\mathrm{CH_3CN})\mathrm{NaCuL}^{\mathrm{dpen(1R2R)}}]_{1\infty}$, in which within a chain two adjacent molecules with the same chirality are linked by a $\mathrm{Na^+}$ ion to form a homochiral chain. The assembly reaction of the racemic mixture $\{\mathrm{Cu^{II}L^{dpen(1R2R/1S2S)}}\}^-$ as donor component with $\mathrm{Na^+}$ ion as acceptor component in $\mathrm{CH_3CN}$ generates a homochiral chain and the adjacent two chains with opposite chiralities of $[(CH_3CN)NaCuL^{dpen(1R2R)}]_{1\infty}$ and $[(CH_3CN)NaCuL^{dpen(1S2S)}]_{1\infty}$ are stacked alternately and coexist in a crystal. It demonstrates that the assembly reactions of the racemic mixture and the chiral component with Na^+ ion give the similar homochiral chainlike assembly structure. It demonstrates that the definitely different assembly structures have not been obtained using the Na^+ ion as the acceptor component.

Circular Tetranuclear Structure of $[Cu^{II}L^{dpen(1R2R/1S2S)}$-$Ln^{III}(NO_3)_2]_2$ (1Gd, 1Tb, 1Dy). The assembly reaction of the racemic copper(II) complex $Na[Cu^{II}L^{dpen(1R2R/1S2S)}]$-$\cdot H_2O\cdot 0.5CH_3CN$ and $Ln^{III}(NO_3)_3\cdot 6H_2O$ (Ln^{III} = Gd^{III}, Tb^{III}, Dy^{III}) in acetonitrile produced plate crystals of $[Cu^{II}L^{dpen(1R2R)}Ln^{III}(NO_3)_2(CH_3CN)]_2$ (**1Gd**, **1Tb**, and **1Dy** for Ln^{III} = Gd^{III}, Tb^{III}, and Dy^{III}). **1Gd** crystallizes as dark gray plate crystals in a centrosymmetric triclinic space group *P*-1 (No. 2). **1Tb** and **1Dy** crystallize as blue-green plate crystals in a centrosymmetric monoclinic space group $P2_1/n$ (No. 14). Table 3 shows the X-ray crystallographic data for **1Gd, 1Tb,** and **1Dy**. Table 4 shows their relevant bond distances and angles; Figures 5(a) and (b) show the centrosymmetric circular $[Cu^{II}{}_2Ln^{III}{}_2]$ structures of **1Gd** and **1Tb** with the selected atom numbering scheme.

Though these three complexes are not isomorphous to each other, they have a similar circular tetranuclear structure to **1Gd**. The structure of **1Gd** is described in detail. The crystallographic unique unit consists of one of $[Cu^{II}L^{dpen(1R2R)}Gd^{III}(NO_3)_2]$ and $[Cu^{II}L^{dpen(1S2S)}Gd^{III}(NO_3)_2]$, where the two enantiomorphs are related by an inversion center. In the binuclear structure of $[Cu^{II}L^{dpen(1R2R)}Gd^{III}(NO_3)_2]$ or $[Cu^{II}L^{dpen(1S2S)}Gd^{III}(NO_3)_2]$, the Cu^{II} and Gd^{III} ions are bridged by the two phenoxo oxygen atoms of $Cu^{II}L^{dpen(1R2R)}$ or $Cu^{II}L^{dpen(1S2S)}$ with Gd−Cu = 3.370(1) Å. Two di-μ-phenoxo-bridged $[Cu^{II}Gd^{III}]$ units, $[Cu^{II}L^{dpen(1R2R)}Gd^{III}(NO_3)_2]$ and $[Cu^{II}L^{dpen(1S2S)}Gd^{III}(NO_3)_2]$, with opposite chiralities are linked by amido oxygen atoms O3 and O3*, with Gd−O3* = 2.267(7) Å (*; 1−x, 1−y, 1−z) to form a circular $[Cu^{II}{}_2Gd^{III}{}_2]$ structure with Gd−Cu* = 5.627(1) Å. The Cu^{II} ion has a square planar coordination geometry and the equatorial coordination sites are occupied by N_2O_2 donor atoms of the electronically trinegative ligand $L^{dpen(1R2R)}$ or $Cu^{II}L^{dpen(1S2S)}$. Gd^{III} ion has an octacoordination geometry with O_8 oxygen atoms, consisting of the four oxygen atoms of two NO_3^- ions as bidentate chelate ligands and three oxygen atoms as a tridentate “ligand-complex,” $Cu^{II}L^{dpen(1R2R)}$ or $Cu^{II}L^{dpen(1S2S)}$ in a binuclear unit, and an amido oxygen atom as a monodentate ligand from the other “ligand complex.” The $Gd^{III}O_8$ coordination geometry is best described as a triangular dodecahedron (TDD) by SHAPE analysis.[20] whose result is given in supplementary data S3. The angles of the bridging CuO_2Gd core of the binuclear unit are Cu−O1−Gd = 103.66(19)° and Cu−O2−Gd = 104.71(19)°. The amido-bridge gives the angle of Gd−O3*−C7* = 133.9(5)°.

Figure 5(b) shows the centrosymmetric circular $[Cu^{II}{}_2Tb^{III}{}_2]$ structure similar to **1Gd**. The crystallographic unique unit consists of half of the $[Cu^{II}{}_2Tb^{III}{}_2]$ structure, where two enantiomorphs, $[Cu^{II}L^{dpen(1R2R)}(H_2O)Tb^{III}(NO_3)_2]$ and $[Cu^{II}L^{dpen(1S2S)}(H_2O)$-$Tb^{III}(NO_3)_2]$, related by an inversion center are linked by amido oxygen atoms O3 and O3*−Tb−O3* and Tb*−O3 = 2.2249(13) Å (*; 1−x, 1−y, −z) to form a circular $[Cu^{II}Tb^{III}]_2$ structure with Tb−Cu* = 5.7174(3) Å. The noteworthy difference from **1Gd** is found in the coordination geometry of the Cu^{II} ion. The Cu^{II} ion has a square pyramidal coordination geometry, and the axial coordination site is occupied by the oxygen atom of a water molecule with Cu−O11 = 2.4146(16) Å for **1Tb**, and by the nitrogen atom of acetonitrile with Cu−N5 = 2.413(3) Å for **1Dy**. The pale reddish color of **1Gd** is ascribed to the square planar coordination geometry of the Cu^{II} ion, and the green color of **1Tb** and **1Dy** is ascribed to the square pyramidal coordination geometry, on the basis of the results of a number of Cu^{II} complexes with similar N_2O_2 tetradentate Schiff-base ligands.[21]

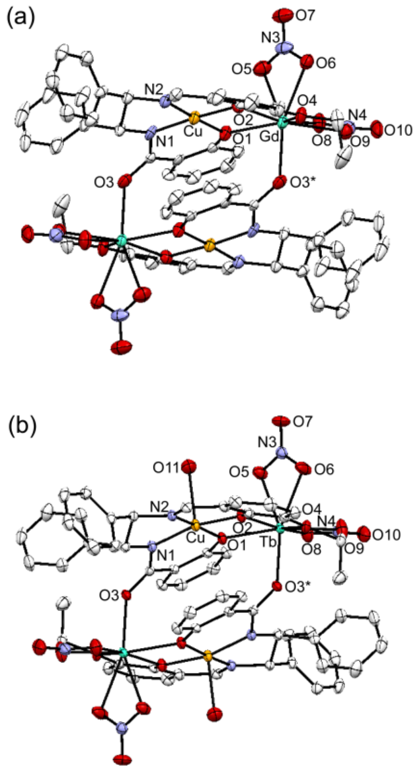

Figure 5. (a) Centrosymmetric circular structure of $[Cu^{II}L^{dpen(1R2R/1S2S)}Gd^{III}(NO_3)_2]_2$ (**1Gd**) and (b) $[Cu^{II}L^{dpen(1R2R/1S2S)}(H_2O)Tb^{III}(NO_3)_2]_2$ (**1Tb**). For **1Tb**, the axial coordination site of Cu^{II} ion is occupied by the oxygen atom of a water molecule O11.

Chainlike Structure of $[Cu^{II}L^{dpen(1R2R)}Ln^{III}(NO_3)_2$-$(CH_3CN)]_{1\infty}\cdot CH_3CN$ (2Gd, 2Tb, 2Dy). The assembly reaction of the optically pure copper(II) complex $Na[Cu^{II}L^{dpen(1R2R)}]\cdot H_2O$ and $Ln^{III}(NO_3)_3\cdot 6H_2O$ (Ln^{III} = Gd^{III}, Tb^{III}, Dy^{III}) in acetonitrile produced red block crystals of $[Cu^{II}L^{dpen(1R2R)}Ln^{III}(NO_3)_2(CH_3CN)]_{1\infty}$, (**2Gd**, **2Tb**, and **2Dy**). They crystallized into a chiral orthorhombic space group $P2_12_12_1$ (No. 19) with similar cell dimensions. Table 3 shows the X-ray crystallographic data for **2Gd, 2Tb,** and **2Dy**. Table 4 shows their relevant bond distances and angles.

As the three compounds have an isomorphous structure, the structural description of **2Gd** is described. The 1D structure of **2Gd** with the relevant atom numbering is shown in Figure 6. The crystallographic unique unit consists of $[Cu^{II}L^{dpen(1R2R)}Ln^{III}(NO_3)_2(CH_3CN)]$ and one acetonitrile as the crystal solvent, in which the Cu^{II} and Gd^{III} ions are bridged by two phenoxo oxygen atoms of $Cu^{II}L^{dpen(1R2R)}$, with Gd−Cu = 3.3348(9) Å, to form a binuclear $[Cu^{II}Gd^{III}]$ unit. Two adjacent $[Cu^{II}Gd^{III}]$ units with same chirality are related by a symmetry operation (*; 1−x, −1/2+y, 1/2−z) and are linked by an amido oxygen atom with the Gd−O3* = 2.228(5) Å, and the linkage is repeated to form a 1D structure running along the *b*-axis of $[Cu^{II}L^{dpen(1R2R)}Gd^{III}(NO_3)_2(CH_3CN)]_{1\infty}$, with Gd−Cu* = 6.2326(9) Å.

The Cu^{II} ion has a square planar coordination geometry with N_2O_2 donor atoms of the asymmetrical tetradentate ligand $L^{dpen(1R2R)}$, and the red color is due to the square planar coordination geometry around the Cu^{II} ion. The Gd^{III} ion has a nonacoordinate geometry with NO_8 donor atoms, consisting of the nitrogen atom of the acetonitrile molecule with the Gd−N5 = 2.570(7) Å, four oxygen atoms of two NO_3^- ions as bidentate chelate ligands, three oxygen atoms as a tridentate "ligand-complex" at one side, and an amido oxygen atom as a monodentate ligand at the opposite side. The $Gd^{III}NO_8$ coordination geometry is best described as a muffin (MFF) by SHAPE analysis, while the circular tetranuclear complex **1Gd** has an octacoordinate geometry with $Gd^{III}O_8$ and is best described as a triangular dodecahedron (TDD).[20] The angles of the bridging CuO_2Gd core are Cu−O1−Gd = 99.26(18)° and Cu−O2−Gd = 103.4(2)°, whose values are smaller than the corresponding values of Cu−O1−Gd = 103.66(19)° and Cu−O2−Gd = 104.71(19)° of **1Gd**. The amido-bridge gives the angle of Gd−O3*−C7* = 177.6(4)°, which is larger than the corresponding value of Gd−O3*−C7* = 138.82(12)° of the circular tetranuclear complex **1Gd**.

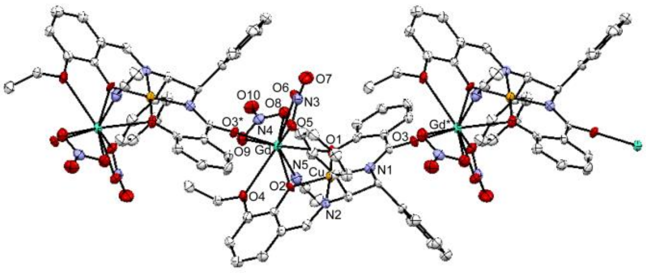

Figure 6. One-dimensional chain structure of $[Cu^{II}L^{dpen(1R2R)}$-$Gd^{III}(NO_3)_2(CH_3CN)]_{1\infty}$, where the phenoxo-bridged binuclear $[Cu^{II}Gd^{III}]$ units are alternately linked through the amido oxygen to form a chainlike structure along the *b*-axis.

General Procedure of Magnetic Measurements. The temperature dependences of the magnetic susceptibilities for the two series of $Cu^{II}Ln^{III}$ complexes (**1Ln**) and (**2Ln**) were measured on powdered samples dispersed in paraffin at a temperature range of 1.9−300 K under 0.5 T. The field dependences of the magnetization with and without liquid paraffin were measured at 1.9 K from 0 to 5 *T*. The ac magnetic susceptibilities were measured as a function of the temperature from 2 to 20 K under 0, 1000, and 2000 Oe applied dc field and 5 Oe oscillating field at frequencies ranging from 10 to 10000 Hz. The experimental magnetic susceptibility $\chi_{3d\text{-}4f}$ can be compared with the values for one 3d and one 4f noninteracting ions, χ_{3d} and χ_{4f}, which can be evaluated by equations (1) and (2), respectively.

$$\chi_{3d} = (Ng^2\beta^2/3kT)[S(S+1)] \quad (1)$$

$$\chi_{4f} = (Ng_J{}^2\beta^2/3kT)[J(J+1)], \quad g_J = 3/2 + [S(S+1) - L(L+1)]/2J(J+1) \quad (2)$$

Circular Tetranuclear $(Cu^{II}Gd^{III})_2$ 1Gd and Chainlike $(Cu^{I}Gd^{III})_{1\infty}$ 2Gd. The magnetic behaviors of **1Gd** and **2Gd** are shown as the plots of $\chi_M T$ versus *T* and $1/\chi_M$ versus *T* in Figure 7(a), where χ_M is the molar magnetic susceptibility per $Cu^{II}Gd^{III}$ and *T* is the absolute temperature. The $\chi_M T$ values for **1Gd** and **2Gd** at 300 K are 8.84 and 8.37 cm^3 K mol^{-1}, respectively. These values are comparable to each other and slightly larger than the calculated value of 8.25 cm^3 K mol^{-1} expected for one Cu^{II} (S = 1/2) and one Gd^{III} ($4f^7$, J = 7/2, L = 0, S = 7/2, $^8S_{7/2}$) noninteracting ions. The plots of $1/\chi_M$ versus *T* for **1Gd** and **2Gd** follow the Curie-Weiss equation ($1/\chi_M = (T-\theta)/C$), with Weiss constants of θ = +2.8 K and θ = +3.0 K, respectively, clearly indicating ferromagnetic interaction.

Upon lowering the temperature, the $\chi_M T$ value of **1Gd** increases gradually to reach a maximum value of 14.00 cm^3 K mol^{-1} at 4.0 K and then decreases abruptly to 11.83 cm^3 K mol^{-1} at 1.9 K. The maximum value of $\chi_M T$ is larger than the value of 9.85 cm^3 K mol^{-1} expected for isolated S = 4 spins resulting from ferromagnetic coupling between the Cu^{II} (S =1/2) and Gd^{III} (S =7/2) ions of the dinuclear unit, but is also smaller than 18.0 cm^3 K mol^{-1} expected for half of the S = 8 spin state of the fully ferromagnetically coupled $Cu^{II}_2Gd^{III}_2$ spin system. The abrupt decrease in $\chi_M T$ in the lower-temperature region can be ascribed to a weak intra- and/or intermolecular antiferromagnetic interaction.

The profiles of $\chi_M T$ versus *T* plots of **2Gd** show a significant difference from **1Gd** in the lowest-temperature region. The $\chi_M T$ value of **2Gd** increases monotonically to become 20.65 cm^3 K mol^{-1} at 1.9 K. The increase in the $\chi_M T$ value indicates the occurrence of a ferromagnetic interaction between Cu^{II} and Gd^{III} ions. The largest value of $\chi_M T$ = 20.65 cm^3 mol^{-1} K at 1.9 K is larger than 9.85 cm^3 mol^{-1} K expected for an S = 4 spin state resulting from ferromagnetic coupling between Cu^{II} (S = 1/2) and Gd^{III} (S = 7/2) in a dinuclear Cu^{II}-Gd^{III} unit and is even larger than 18.0 cm^3 mol^{-1} K expected for an $S = 8 \times 1/2$ spin state in a ferromagnetically coupled tetranuclear Cu^{II}–Gd^{III}–Cu^{II}–Gd^{III} unit.

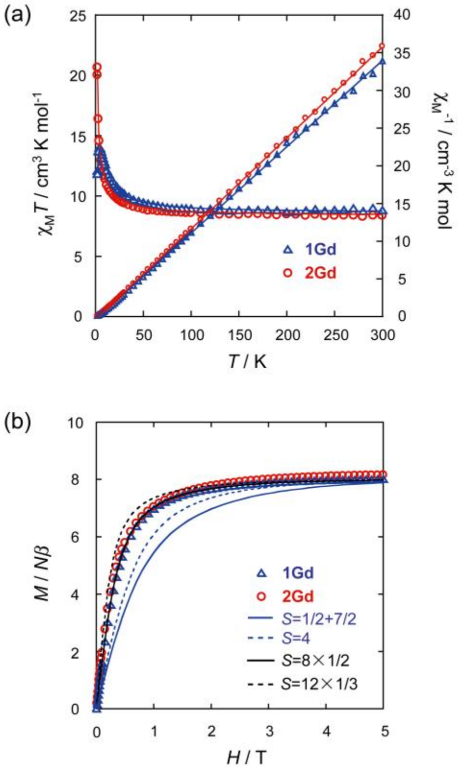

Figure 7. (a) Plots of $\chi_M T$ versus *T* and $1/\chi_M$ versus *T* for **1Gd** (blue triangle) and **2Gd** (red circle), where χ_M is the molar magnetic susceptibility per CuGd. The blue solid line for **1Gd** in $\chi_M T$ versus *T* curve represents the theoretical curve with the parameters g_{Cu} = 2.31, g_{Gd} = 2.03, J_1 = +4.6 cm^{-1}, J_2 = +1.8 cm^{-1}, and zJ'= –0.013 cm^{-1}. The red solid line for **2Gd** in the $\chi_M T$ versus *T* curve represents the theoretical curve derived from the spin Hamiltonian based on the chain structure with parameters g_{Cu} = 2.21, g_{Gd} = 2.00, J_1 = +4.2 cm^{-1}, J_2 = +0.037 cm^{-1}. (b) Field dependence of the magnetization up to 5 T of **1Gd** (red circle) and **2Gd** (blue triangle) at 1.9 K as plots of $M/N\beta$ versus *H*, where the magnetization *M* is the value per CuGd. The experimental $M/N\beta$ value is much higher than the calculated curves of Brillouin functions expected for magnetically isolated one Cu^{II} (S = 1/2) and one Gd^{III} ($4f^7$, *J*

$=7/2$, $L = 0$, $S = 7/2$, ${}^8S_{7/2}$) ions (blue solid line) and $S = 4$ expected for the ferromagnetic coupled binuclear CuGd unit (blue dotted line). The calculated curve with the Brillouin function of $S = 8\times1/2$ (($\mathrm{Cu^{II}–Gd^{III}–Cu^{II}–Gd^{III}}$)/2) is drawn in the black solid line.

To reproduce the magnetic susceptibility data of **1Gd** and to evaluate the magnetic interaction parameters, we used the spin-only Hamiltonian (3) based on the circular tetranuclear $\mathrm{Cu^{II}_2Gd^{III}_2}$ structure, whose spin structure is shown in Scheme 2(a).

$$\boldsymbol{H} = g_{\mathrm{Cu}}\beta(S_{\mathrm{Cu1}} + S_{\mathrm{Cu2}})\cdot H + g_{\mathrm{Gd}}\beta(S_{\mathrm{Gd1}} + S_{\mathrm{Gd2}})\cdot H - J_1(S_{\mathrm{Cu1}}S_{\mathrm{Gd1}} + S_{\mathrm{Cu2}}S_{\mathrm{Gd2}}) - J_2(S_{\mathrm{Cu1}}S_{\mathrm{Gd2}} + S_{\mathrm{Cu2}}S_{\mathrm{Gd1}}) \quad (3)$$

In equations (3), g_{Cu} and g_{Gd} are the g-factors for the $\mathrm{Cu^{II}}$ and $\mathrm{Gd^{III}}$ ions, respectively, H is the applied magnetic field, J_1 is the Heisenberg coupling constant between $\mathrm{Cu^{II}}$ and $\mathrm{Gd^{III}}$ ions through two phenoxo monoatomic bridges, and J_2 is the Heisenberg coupling constant between the $\mathrm{Cu^{II}}$ and $\mathrm{Gd^{III}}$ ions through a three-atom N–C=O amido bridge.

Scheme 2. Spin structures for the (a) circular tetranuclear ($\mathrm{Cu^{II}}$-$\mathrm{Gd^{III}}$)$_2$ complex and (b) chainlike ($-\mathrm{Cu^{II}Gd^{III}}-$)$_{1\infty}$ complex.

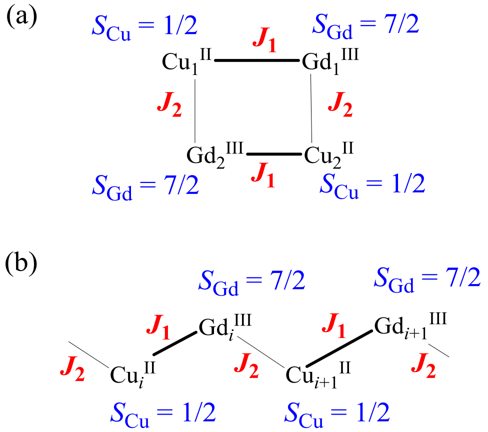

The magnetic susceptibility of **1Gd** at each temperature was calculated using the following theoretical equation (4),

$$\chi = [N\Sigma_i(-\mathrm{d}E_i/\mathrm{d}H)\exp(-E_i/kT)]/[H\Sigma_i\exp(-E_i/kT)] \quad (4)$$

where the energy level, E_i, was evaluated by diagonalizing the Hamiltonian matrix (with dimensions 256 × 256) in the uncoupled spin function basis set. Moreover, a molecular field term $-zJ'\langle S_z\rangle S_z$ was added to the Hamiltonian to describe the molecular interactions between the tetrameric units. The magnetic susceptibility data over the entire range of temperatures of **1Gd** were well reproduced with an agreement factor R as low as 1.1×10^{-4}, and best-fit parameters of $g_{\mathrm{Cu}} = 2.31$, $g_{\mathrm{Gd}} = 2.03$, $J_1 = +4.6\ \mathrm{cm^{-1}}$, $J_2 = +1.8\ \mathrm{cm^{-1}}$, and $zJ' = -0.013\ \mathrm{cm^{-1}}$ were obtained. The theoretical curve is drawn by the blue solid line in Figure 7(a). The positive signs of J_1 and J_2 indicate that ferromagnetic interactions are operating between $\mathrm{Cu^{II}}$ and $\mathrm{Gd^{III}}$ ions, both through the di-μ-phenoxo bridge and the amido Cu–N–C=O–Gd bridge. The magnitudes of the J_1 and J_2 values are in the range of values reported previously for $\mathrm{Cu^{II}Gd^{III}}$ polynuclear complexes with similar di-μ-phenoxo and amido Cu–N–C=O–Gd bridges.[22]

A rigorous analysis of the magnetic susceptibility data of **2Gd** would require the spin-only Hamiltonian (equation (5)) based on the linear chain structure of ($-\mathrm{Cu^{II}}-\mathrm{Gd^{III}}-$)$_{1\infty}$, whose spin structure is shown in Scheme 2(b) and all symbols have the same meaning as in equation (3).

$$\boldsymbol{H} = g_{\mathrm{Cu}}\beta(S_{\mathrm{Cu1}} + S_{\mathrm{Cu2}})\, H + g_{\mathrm{Gd}}\beta(S_{\mathrm{Gd1}} + S_{\mathrm{Gd2}})\cdot H - \Sigma_i(J_1S_{\mathrm{Cu}i}\, S_{\mathrm{Gd}i} + J_2S_{\mathrm{Gd}i}\, S_{\mathrm{Cu}i+1}) \quad (4)$$

Because of the complexity of such a Hamiltonian, a quantitative evaluation of the magnetic interaction parameters J_1 and J_2 is possible only resorting to drastic approximations. We will employ a previously proposed "chain of dimers" model, where strongly coupled di-μ-phenoxo bridged $\mathrm{Cu^{II}Gd^{III}}$ dimers are assumed to act as effective S_{d} classical spin systems weakly interacting along the chain through the amido bridges.[23] The effective S_{d} spin can be obtained as

$$S_{\mathrm{d}} = ½\,\{-1 + [1 + 4\chi_{\mathrm{d}}T/(0.1251g^2)]^{1/2}\},$$

where g is the average g-value and χ_{d} is the susceptibility per $\mathrm{Cu^{II}Gd^{III}}$ dimer, given by:

$$\chi_{\mathrm{d}}T = (4N\beta/k_{\mathrm{B}})[15g_4^2+7g_3^2\exp(-4J_1/k_{\mathrm{B}}T)]/[9+7\exp(-4J_1/k_{\mathrm{B}}T)],$$

where $g_4 = (7g_{\mathrm{Gd}} + g_{\mathrm{Cu}})/8$ is the g-value associated with the lowest lying $S = 4$ level and $g_3 = (9g_{\mathrm{Gd}} - g_{\mathrm{Cu}})/8$ is the g-value associated to the highest $S = 3$ level.

The final susceptibility for the infinite chain of classical spins, χ_{chain}, can be obtained according to the Fisher's model[24] using the Drillion function[25] as

$$\chi_{\mathrm{chain}} = [N\beta^2g^2S_{\mathrm{d}}(S_{\mathrm{d}} + 1)/3k_{\mathrm{B}}T](1 + u)/(1 - u)$$
$$u = \coth[2J_2S_{\mathrm{d}}(S_{\mathrm{d}} + 1)/k_{\mathrm{B}}T] - [k_{\mathrm{B}}T/2J_2S_{\mathrm{d}}(S_{\mathrm{d}} + 1)],$$

where J_2 is the interdimer coupling constant.

A least square fitting of the experimental data gave the following parameters: $g_{\mathrm{Cu}} = 2.21$, $g_{\mathrm{Gd}} = 2.00$, $J_1 = +4.2\ \mathrm{cm^{-1}}$, and $J_2 = +0.037\ \mathrm{cm^{-1}}$. The coupling constants through two phenoxo bridges and a three-atom N-C=O bridge, J_1 and J_2, are both positive, and the J_1 value is larger than the J_2 value. This result is in accord with analogous $\mathrm{Cu^{II}Gd^{III}}$ complexes with this type of bridging ligand.[22] It is noteworthy that the magnitude of J_2 value for **2Gd** is smaller than that of **1Gd**.

The field dependence of the magnetization up to 5 T at 1.9 K is shown in Figure 8 as the plots of $M/N\beta$ vs. H for **1Gd** (blue triangle) and **2Gd** (red circle). These experimental data are much higher than the calculated curve of Brillouin functions expected for magnetically isolated one $\mathrm{Cu^{II}}$ ($S = 1/2$) and one $\mathrm{Gd^{III}}$ ($4f^7$, $J = 7/2$, $L = 0$, $S = 7/2$, ${}^8S_{7/2}$) ions (blue solid line) as well as $S = 4$ (blue dotted line), whose spin ground state is expected for the binuclear CuGd unit resulting from the $\mathrm{Cu^{II}}$–$\mathrm{Gd^{III}}$ ferromagnetic coupling. The experimental data for **1Gd** is rather close to the theoretical curve obtained for $S = 8$ (black solid line), resulting from the ferromagnetic coupling of all of the $\mathrm{Cu^{II}}$ and $\mathrm{Gd^{III}}$ ions within the tetrameric complex. A very good fit could be obtained for $g = 2.01$ (see solid line in Figure 8). The experimental data of **2Gd** is rather close to the theoretical curve of $S = 8\times1/2$, whose spin ground state is the result of ferromagnetic coupling of $\mathrm{Cu^{II}–Gd^{III}–Cu^{II}–Gd^{III}}$ and is lower than the theoretical curve of $S = 12\times1/3$ (black dotted line), whose spin ground states can be the result of the ferromagnetic coupling of ($-\mathrm{Cu^{II}}-\mathrm{Gd^{III}}-$)$_3$. The magnetization and magnetic susceptibility data demonstrate that the 1D complex $[\mathrm{Cu^{II}L^{dpen(1R2R)}Gd^{III}(NO_3)_2(CH_3CN)}]_{1\infty}$ is a ferromagnetic chain.

Circular Tetranuclear ($\mathrm{Cu^{II}Tb^{III}}$)$_2$ and Chainlike ($\mathrm{Cu^{II}Tb^{III}}$)$_{1\infty}$ Complexes 1Tb and 2Tb. Figure 8(a) shows the plots of $\chi_{\mathrm{M}}T$ versus T. The $\chi_{\mathrm{M}}T$ values at 300 K are 12.75 and 12.31 $\mathrm{cm^3\ K\ mol^{-1}}$ for **1Tb** and **2Tb**, respectively. These are slightly larger than the value of 12.19 $\mathrm{cm^3\ K\ mol^{-1}}$ expected for noninteracting ions of $\mathrm{Cu^{II}}$ ($S = 1/2$) and $\mathrm{Tb^{III}}$ ($4f^8$, $J = 6$, $S = 3$, $L = 3$, ${}^7F_6$) with $g_{\mathrm{Cu}} = 2$ and $g_J = 3/2$. Upon lowering the temperature, the $\chi_{\mathrm{M}}T$ value decreases, reaching shallow bottom of 12.29 $\mathrm{cm^3\ K\ mol^{-1}}$ at 80 K and 10.30 $\mathrm{cm^3\ K\ mol^{-1}}$ at 30 K, and then increases to 21.53 and 15.69 $\mathrm{cm^3\ K\ mol^{-1}}$ at 1.9 K for **1Tb** and **2Tb**, respectively. The decrease is mainly due to the crystal field effect on the $\mathrm{Tb^{III}}$ ion (Stark splitting),[13] while the increase in the $\chi_{\mathrm{M}}T$ value at the low-temperature region can be ascribed to weak intramolecular $\mathrm{Cu^{II}}$-$\mathrm{Tb^{III}}$ ferromagnetic interactions.[14] Two kinds of magnetic interaction between Cu^{II} and Tb^{III} ions can be identified in both **1Tb** and **2Tb**: the J_1 of intradimer interaction via two phenoxo bridges and a supposedly weaker J_2 of interdimer interaction via an amido bridge. At present, magnetic calculation has not been applied to estimate the magnetic coupling constants due to the intrinsic magnetic anisotropy of the Tb^{III} ion. The distinct different magnetic profiles in the $\chi_M T$ versus T plots can be mainly ascribed to the difference in the interdimer magnetic interaction via the amido-bridge for two compounds. The limited decrease in $\chi_M T$ with respect to the room temperature value and the steep increase below 80 K suggest that for **1Tb**, both J_1 and J_2 are positive. In contrast, the more discernible decrease in $\chi_M T$ and the modest increase only below 30 K suggest that for the 1D complex **2Tb**, J_1 is significantly positive, while J_2 is very weak or even negligible. This difference could be related to the different bridging geometries observed in the X-ray structure analyses: Tb−O3*−C7* = 138.82(12)° and 177.0(3)° (* indicate the corresponding atoms of the neighboring dimeric unit) for **1Tb** and **2Tb**, respectively.

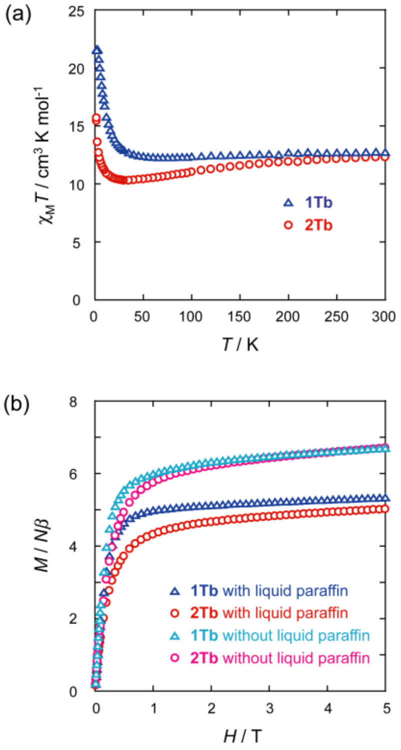

Figure 8. (a) Temperature dependence of magnetic susceptibility for **1Tb** (blue) and **2Tb** (red) in the form of $\chi_M T$ versus T plots. (b) Field dependence of magnetization at 1.9 K with and without liquid paraffin for **1Tb** (blue) and **2Tb** (red). The magnetization profiles with liquid paraffin are drawn by deep colors and those without liquid paraffin are drawn by pale colors.

The field-dependent magnetizations from 0 to 5 T were measured at 1.9 K by using samples with and without liquid paraffin, and the results are shown in Figure 8(b) in the form of $M/N\beta$ versus H plots, where the magnetization is the value per CuTb. Upon increasing the applied external magnetic field, the magnetization of **1Tb** and **2Tb** with liquid paraffin increases to 5.34 and 5.01 $N\beta$ at 5 T without reaching the expected saturation value of 10 $N\beta$ (9 $N\beta$ for Tb^{III} ion and 1 $N\beta$ for each of Cu^{II} ion). This is mostly due to the crystal field effect on the Tb^{III} ion ($4f^8$, J = 6, S = 3, L = 3, $^7F_6$) that removes the 13-fold degeneracy of the $^7F_6$ ground state. The magnetization of **1Tb** increases more rapidly in the weak applied magnetic field than **2Tb**. The magnetization of **1Tb** and **2Tb** without liquid paraffin increases to 6.70 $N\beta$ at 5 T, which are considerably larger than the corresponding values with liquid paraffin. This behavior indicates the presence of strong magnetic anisotropy in **1Tb** and **2Tb**.

Dynamics properties of **1Tb** and **2Tb** were examined by ac magnetic susceptibility measurements at frequencies of 10−10,000 Hz as a function of temperature at 2−10 K. **1Tb** showed a frequency dependence of ac magnetic susceptibility, and the maximums of χ_M' and χ_M'' were observed under zero external dc magnetic field (Figure 9(a)). This indicates relatively slow relaxation of magnetization. The Arrhenius plot shows a straight line for the $\chi_{M''}$ peak (Fig. 10), and the activation energy (Δ) for the magnetization reversal under zero magnetic field was estimated as Δ/k_B = 29.4(6) K with τ_0 = 1.5(3) $\times 10^{-8}$ s, where τ_0 stands for the pre-exponential factor in the Arrhenius equation, $\ln(2\pi\nu) = -\ln(\tau_0) - \Delta/k_B T$.[15b] The Cole-Cole analysis[26] was performed for **1Tb** using the above AC susceptibilities and the equation $\chi(\omega) = \chi_S + (\chi_T - \chi_S)/(1 + (i\omega\tau)^{1-\alpha})$, where χ_T and χ_S are the isothermal and adiabatic magnetic susceptibilities, respectively.[27] The plot draws a partial semicircle (Fig. S2, Supporting Information), and the optimized α value was 0.093(3) at 3.0 K. This finding indicates a relaxation process operative in **1Tb**. **2Tb** showed an only slight χ_M'' without any external dc field (Figure 9(b1)), but the frequency dependency of ac magnetic susceptibility was pronounced at an external magnetic field of 1000 Oe (Figure 9(b2)). From these data, it can be concluded that the Arrhenius plot exhibited a straight line (Fig. 10), and the parameters were estimated as Δ/k_B = 20.6(3) K and τ_0 = 2.9(3) $\times 10^{-9}$ s for **2Tb**. The Cole-Cole analysis gave a semicircle (Fig. S2, Supporting Information), and the optimized α value was determined to be 0.39(1) at 2.0 K. Here, the external field was applied only for suppressing the zero-field quantum tunneling of magnetization (QTM).[27]

The Arrhenius parameters for **1Tb** and **2Tb** are comparable to each other, indicating that the slow magnetic reversal comes from a similar origin. As previously described, the interdimer magnetic interaction through an amido group in **2Tb** is negligibly small. Thus, the slow magnetic reversal may come from $Cu^{II}Tb^{III}$ dimeric species.

1Tb showed frequency dependence of ac magnetic susceptibility under zero external dc magnetic field, while **2Tb** showed no frequency dependence under a zero external magnetic field, but showed a meaningful frequency dependence under an external magnetic field. The isolated binuclear Cu^{II}-Tb^{III} complexes with the similar bridging groups $[Cu^{II}(L)(O_2COMe)Tb^{III}(thd)_2]$[18b] (L = *N,N'*-bis(3-methoxy-2-oxybenzylidne-2,2'-dimethylpropylamine) and $[Cu^{II}(3\text{-MeOsaltn})(ac)Tb^{III}(hfac)_2]$[14a] ($H_2$(3-MeOsaltn) = *N,N'*-bis(3-methoxy-2-oxybenzylidene)-1,3-propanediamine, ac = acetate, hfac = hexafluoroacetylacetonato) behave as field-induced SMMs behavior. When the interdimer magnetic interaction of **2Tb** was improved by the modification of the steric effect of the ligand, the pronounced magnetic property of SCM would appear.

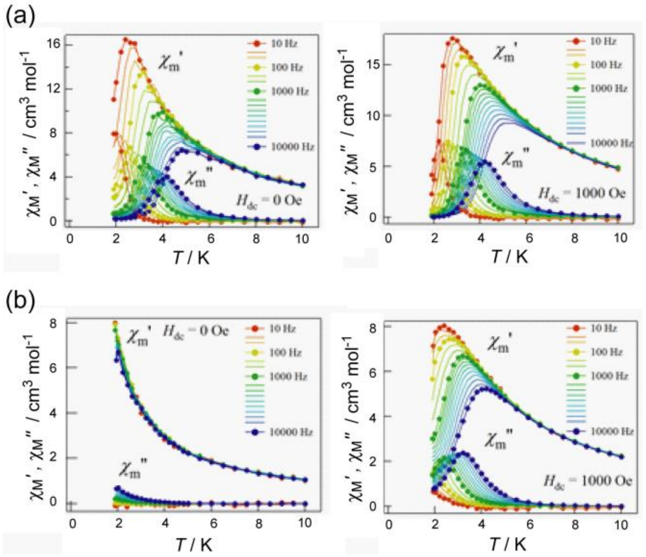

Figure 9. (a) Temperature dependences of the in-phase (χ_M') and out-of phase (χ_M'') ac susceptibility signals of **1T**b and **2Tb** measured under various frequencies and under 0 and 1000 Oe external direct current fields.

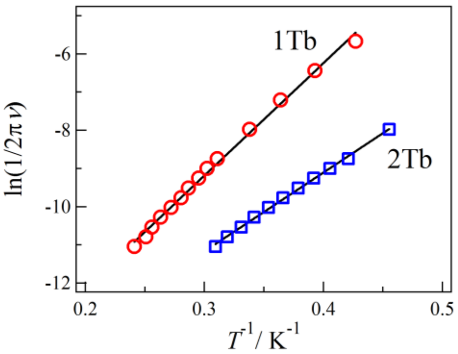

Figure 10. Arrhenius plot of **1Tb** measured without any external dc field and **2Tb** measured at an external dc field of 1000 Oe.

Circular Tetranuclear ($Cu^{II}Dy^{III}$)$_2$ and Chainlike ($Cu^{II}Dy^{III}$)$_{1\infty}$ Complexes 1Dy and 2Dy. Figure 11(a) shows the plots of $\chi_M T$ versus T. The $\chi_M T$ values at 300 K are 14.53 and 14.29 cm^3 K mol^{-1} for **1Dy** and **2Dy**, respectively. These values are slightly smaller than the value of 14.55 cm^3 K mol^{-1} expected for noninteracting ions of Cu^{II} (S = 1/2) and Dy^{III} ($4f^9$, J = 15/2, S = 5/2, L = 5, $^6H_{15/2}$) with g_{Cu} = 2 and g_J = 4/3. Upon lowering the temperature, the $\chi_M T$ value decreases, reaching shallow bottom values of 13.85 cm^3 K mol^{-1} at 60 K and 11.41 cm^3 K mol^{-1} at 18 K, and then increases to 23.79 and 12.07 cm^3 K mol^{-1} at 1.9 K for **1Dy** and **2Dy**, respectively. The decrease is mainly due to the crystal field effect on the Dy^{III} ion (Stark splitting),[13] while the increase in the $\chi_M T$ value at the low-temperature region can be ascribed to weak intramolecular Cu^{II}-Dy^{III} ferromagnetic interactions.[14] Two kinds of magnetic interaction between Cu^{II} and Dy^{III} ions can be identified in both **1Dy** and **2Dy**: the J_1 of intradimer interaction via two phenoxo bridges and a supposedly weaker J_2 of interdimer interaction via an amido bridge. At present magnetic calculation has not been applied to estimate the magnetic coupling constants due to the intrinsic magnetic anisotropy of the Dy^{III} ion. The distinct different magnetic profiles in the $\chi_M T$ versus T plots can be mainly ascribed to the difference in the interdimer magnetic interaction via the amido-bridge for two compounds. The limited decrease in $\chi_M T$ with respect to the room temperature value and the steep increase below 60 K suggest that for **1Dy**, both J_1 and J_2 are positive. In contrast, the more discernible decrease in $\chi_M T$ and the modest increase only below 18 K suggest that for the 1D complex **2Dy,** J_1 is significantly positive, while J_2 is very weak or even negligible. This difference could be related to the different bridging geometries observed in the X-ray structure analyses: Dy−O3*=C7* = 132.22(18)° and 177.1(6)° (* indicate the corresponding atoms of the neighboring dimeric unit) for **1Dy** and **2Dy**, respectively.

The field-dependent magnetizations from 0 to 5 T were measured at 1.9 K by using samples with and without liquid paraffin, and the results are shown in Figure 12(b) in the form of $M/N\beta$ versus H plots, where the magnetization is the value per CuDy. Upon increasing the applied external magnetic field, the magnetization of **1Dy** and **2Dy** with liquid paraffin increases to 5.89 and 5.50 $N\beta$ at 5 T without reaching the expected saturation value of 11 $N\beta$ (10 $N\beta$ for Dy^{III} ion and 1 $N\beta$ for each of Cu^{II} ion). This is mostly due to the crystal field effect on the Dy^{III} ion ($4f^9$, J = 15/2, S = 5/2, L = 5, $^6H_{15/2}$) that removes the 16-fold degeneracy of the $^6H_{15/2}$ ground state. The magnetization of **1Dy** increases more rapidly in the weak applied magnetic field than **2Dy**. The magnetization of **1Dy** and **2Dy** without liquid paraffin increases to 9.47 $N\beta$ and 6.75 $N\beta$ at 5 T, which are considerably larger than the corresponding values with liquid paraffin. This behavior indicates the presence of strong magnetic anisotropy in **1Dy** and **2Dy**.

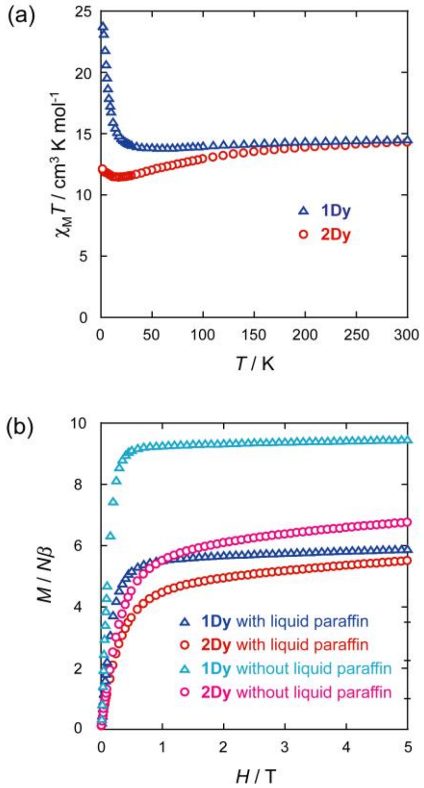

Figure 11. (a) Temperature dependence of magnetic susceptibility for **1Dy** (blue) and **2Dy** (red) in the form of $\chi_M T$ versus T plots. (b) Field dependence of magnetization at 1.9 K with and without liquid paraffin for **1Dy** (blue) and **2Dy** (red). The magnetization profiles with liquid paraffin are drawn by deep colors and those without liquid paraffin are drawn by pale colors.

Dynamics properties of **1Dy** and **2Dy** were examined by ac magnetic susceptibility measurements at frequencies of 10−10,000 (10, 21, 46, 100, 215, 464, 1000, 1291, 1668, 2154, 2782, 3593, 4641, 5994, 7742, 10000) Hz as a function of temperature at 2−25 K under 0, 1000, and 2000 Oe for **1Dy** and under 0 and 1000 Oe for **2Dy**. **1Dy** showed a frequency dependence of ac magnetic susceptibility, and the maximums of χ_M' and χ_M''

were observed under zero external dc magnetic field (Figure 12(a)). This indicates relatively slow relaxation of magnetization. The Arrhenius plot shows a straight line for the $\chi_{M''}$ peak (Figure 13), and the activation energy (Δ) for the magnetization reversal under zero magnetic field was estimated as Δ/k_B =19.5 K with τ_0 = 1.8 $\times 10^{-8}$ s, where τ_0 stands for the pre-exponential factor in the Arrhenius equation, $\ln(2\pi\nu) = -\ln(\tau_0) - \Delta/k_BT$.[15b] The Cole-Cole analysis[10] was performed for **1Dy** using the above ac susceptibilities and the equation, $\chi(\omega) = \chi_S + (\chi_T - \chi_S)/(1 + (i\omega\tau)^{1-\alpha})$, where χ_T and χ_S are the isothermal and adiabatic magnetic susceptibilities, respectively.[17b] The plot draw a partial semicircle (Figure S5, Supporting Information), and the optimized α value was 0.093(3) at 3.0 K. This finding indicates one relaxation process operative in **1Dy**.

2Dy showed an only slight χ_M" without any external dc field (Figure 13(b)), but the frequency dependency of AC magnetic susceptibility was pronounced at an external magnetic field of 1000 Oe (Figure 12(b)). From these data the Arrhenius plot exhibited a straight line (Figure 13), and the parameters were estimated as Δ/k_B = 17.9 K and τ_0 = 5.1 $\times 10^{-8}$ s for **2Dy**. The Cole-Cole analysis gave a semicircle (Figure S5, Supporting Information), and the optimized α value was determined to be 0.39(1) at 2.0 K. Here, the external field was applied only for suppressing the zero-field quantum tunneling of the magnetization (QTM).[28] The present compounds are concluded to be SMMs.

The Arrhenius parameters for **1Dy** and **2Dy** are comparable to each other, indicating that the slow magnetic reversal comes from a similar origin. The magnetic property of the 1D complex **2Dy** can be ascribed to a binuclear unit, in which the interdimer Cu^{II}-Dy^{III} magnetic interaction via the amido oxygen is negligibly small.

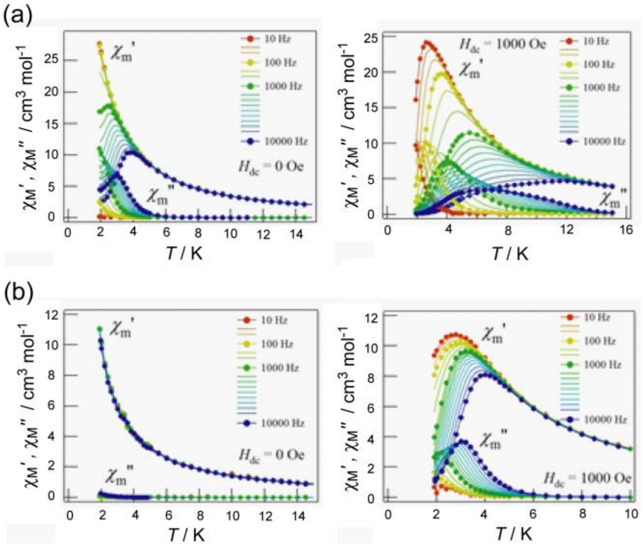

Figure 12. (a) Temperature dependences of the in-phase (χ_M') and out-of phase (χ_M'') ac susceptibility signals of **1Dy** and **2Dy** measured under various frequencies and under 0 and 1000 Oe external direct current fields.

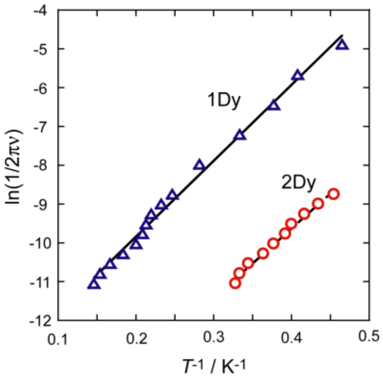

Figure 13. Arrhenius plot of **1Dy** measured without any external dc field and **2Dy** measured at an external dc field of 1000 Oe.

CONCLUSION

The assembly structures of copper(II) components of chiral or racemic ligands ($H_3L^{dpen(1R2R)}$, $H_3L^{dpen(1R2R/1S2S)}$) with Na^+ or Ln^{III} salts ($Ln^{III} = Gd^{III}$, Tb^{III}, Dy^{III}) were studied. The copper(II) component species, $\{Cu^{II}L^{dpen(1R2R)}\}^-$ = (*N*-((1*R*,2*R*)-2-(((*E*)-3-ethoxy-2-oxybenzylidene)amino)-1,2-diphenylethyl)-2-oxybenzamide)-copper(II), functions as a “cross-linking ligand-complex” at the two phenoxo oxygen atoms, one ethoxy oxygen atom, and the amido oxygen atom. The chiral Cu^{II} complex involving a Na^+ ion, $[(CH_3CN)NaCuL^{dpen(1R2R)}]_{1\infty}$, has a chainlike structure, and within a chain, two adjacent molecules with the same chirality are linked by a Na^+ ion to form a homochiral chain structure. The assembly reaction of the racemic mixture $\{Cu^{II}L^{dpen(1R2R/1S2S)}\}^-$ and Na^+ ion in CH_3CN generates a homochiral chainlike structure, and two chains with opposite chiralities of $[(CH_3CN)NaCuL^{dpen(1R,2R)}]_{1\infty}$ and $[(CH_3CN)NaCuL^{dpen(1S,2S)}]_{1\infty}$ coexist in a crystal. It demonstrates that the assembly of racemic species and Na^+ ion gives the same assembly structure as that of the chiral species. The 1:1 assembly reaction of the racemic form of the “cross-linking ligand-complex,” $Na[Cu^{II}L^{dpen(1R2R/1S2S)}]$ and $Ln^{III}(NO_3)_3{\cdot}6H_2O$, gave a centrosymmetric circular $(Cu^{II}Ln^{III})_2$ complex $[Cu^{II}L^{dpen(1R2R/1S2S)}Ln^{III}(NO_3)_2]_2$ (**1Gd**, **1Tb**, **1Dy**), while the reaction of the enantiopure form $Na[Cu^{II}L^{dpen(1R2R)}]$ and $Ln^{III}(NO_3)_3{\cdot}6H_2O$ gave a chiral chainlike $(Cu^{II}Ln^{III})_{1\infty}$ complex $[Cu^{II}L^{dpen(1R2R)}Ln^{III}(NO_3)_2(CH_3CN)]_{1\infty}{\cdot}CH_3CN$ (**2Gd**, **2Tb**, **2Dy**). The magnetic susceptibilities of **1Gd** and **2Gd** were analyzed by the spin-only Hamiltonian based on the circular tetranuclear $(-Cu^{II}Gd^{III}-)_2$ and linear chain $(-Cu^{II}Gd^{III}-)_{1\infty}$ structures, respectively. The Cu^{II}-Gd^{III} magnetic interaction through two phenoxo bridges and a three-atom N−C=O bridge, J_1 and J_2, are both positive, and the magnitude of J_2 value of **2Gd** is extremely smaller than that of **1Gd**. The magnetic susceptibility data of **1Ln** and **2Ln (Ln = Tb, Dy)** showed the crystal field effect on the Ln^{III} ion (Stark splitting). The magnetic properties of **2Tb** and **2Dy** are ascribed to a dimeric unit described as SMM, as the interdimer Cu^{II}-Ln^{III} magnetic interaction via the amido group should be negligibly small due to the substantially different structural geometry at the part from **1Tb**. The magnetizations of **1Ln** and **2Ln (Ln = Tb, Dy)** without liquid paraffin are considerably larger than the corresponding values with liquid paraffin, indicating the presence of strong magnetic anisotropy. **1Tb** and **1Dy** showed frequency dependency of ac magnetic susceptibility under zero external dc magnetic field, indicating the behavior of SMMs. **2Tb** and **2Dy** showed no frequency dependence under zero external magnetic field, but showed a meaningful frequency dependence under an external magnetic field. Their energy barriers of slow magnetic relaxation, Δ/k_B, estimated by the Arrhenius plots are 29.4(6) K and 20.6(3) K for **1Tb** and **2Tb** under zero and 1000 Oe of the dc bias fields, respectively.

EXPERIMENTAL SECTION

Materials. All reagents and solvents in the syntheses were of reagent grade, available from Tokyo Kasei Co., Ltd., Wako Pure Chemical Industries, Ltd., and Fuji Molecular Planning Co., Ltd. These were used without further purification. All reactions were carried out under ambient atmosphere.

Ligands. The racemic and optically pure tetradentate N_2O_2 ligands $H_3L^{dpen(1R2R/1S2S)}$, $H_3L^{dpen(1R2R)}$ $H_3L^{dpen(1S2S)}$ were prepared by a two-step reaction procedure via intermediate product.

***N*-((1*R*,2*R*/1*S*,2*S*)-2-amino-1,2-diphenylethyl)-2-hydroxybenzamide.** This intermediate product was synthesized as follows. (1*R*,2*R*)-1,2-diphenylethylenediamine (1.27 g, 6.0 mmol), (1*S*,2*S*)-1,2-diphenylethylenediamine (1.27 g, 6.0 mmol) and phenylsalicylate (2.57g, 12 mmol) were mixed in a mortar and well ground to be a paste. The paste material was allowed to stand for 9 h in a dry oven at 80 °C. The resulting yellow solid was dissolved in 30 mL of dichloromethane and the yellow solution was separated by silica gel column chromatography (Wakogel® C-200) with 10 cm height and 3 cm diameter. The by-product was removed by eluting 300 mL of dichloromethane, and the desired product was obtained by eluting 120 mL of ethyl acetate. The yellow solution was collected and evaporated to a pale yellow solid. Yield: 2.95 g (74%). ^{1}H NMR (600 MHz, $CDCl_3$, 298 K): δ = 12.2 (OH, br s, 1H), 8.00 (ArH, d, *J* = 7.1 Hz, 1H), 7.58 (ArH, dd, *J* = 1.6 and 7.7 Hz 1H), 7.45-7.44 (ArH, m, 2H), 7.41-7.26 (ArH, NH, m, 9H), 6.94-6.90 (ArH, m, 2H), 5.22 ($\underline{\mathrm{CH}}$-NH, dd, *J* = 2.7 and 7.4 Hz, 1H), 4.52 (CH-N, d, *J* = 2.7 Hz, 1H), 1.58 (NH_2, br s, 2H) ppm. As this intermediate compound is unstable, the next reaction was subsequently performed.

$H_3L^{dpen(1R2R/1S2S)}$, *N*-((1*R*,2*R*/1*S*,2*S*)-2-(((*E*)-3-ethoxy-2-hydroxybenzylidene)amino)-1,2-diphenylethyl)-2-hydroxybenzamide. The intermediate compound (2.95 g, 8.9 mmol) and 3-ethoxysalicylaldehyde (1.48 g, 8.9 mmol) were mixed in 50 mL of methanol and the resulting mixture was warmed on a hot plate for 2 h under stirring. The resulting solution was evaporated to oily material. To the oily material, 30 mL of diethyl ether was added and the solution was stirred for 15 min. Yellow crystalline materials precipitated and were collected by suction filtration. Yield: 2.19 g (51%). Anal. Calcd for $H_3L^{dpen(1R2R/1S2S)}$ = $C_{30}H_{28}N_2O_4$: C, 74.98; H, 5.87; N, 5.83 %. Found: C, 74.68; H, 5.85; N, 5.82%. ^{1}H NMR (500 MHz, $CDCl_3$, 298 K): δ = 11.8 (OH, s, 1H), 8.05 (CH=N, s, 1H), 7.45-7.14 (ArH, OH, NH, m, 14H), 6.98 (ArH, dd, *J* = 1.1 and 7.7 Hz, 1H), 6.93-6.88 (ArH, m, 2H), 6.80 (ArH, dd, *J* = 8.0 and 8.0 Hz, 1H), 6.72 (ArH, dd, *J* = 1.1 and 7.7 Hz, 1H), 5.71 ($\underline{\mathrm{CH}}$-NH, dd, *J* = 3.4 and 8.0 Hz, 1H), 4.84 (CH-N, d, *J* = 2.9 Hz, 1H), 4.16 ($CH_3\underline{CH_2}$, q, *J* = 6.9Hz, 2H), 1.55 ($\underline{CH_3}CH_2$, t, *J* = 6.9 Hz, 3H) ppm. IR (attenuated total reflectance (ATR) method, cm^{-1}): ν(C=N) 1626, ν(C=O) 1589.

***N*-((1*R*,2*R*)-2-amino-1,2-diphenylethyl)-2-hydroxybenzamide.** At the first step, the intermediate product *N*-((1*R*,2*R*)-2-amino-1,2-diphenylethyl)-2-hydroxybenzamide, that is the 1:1 condensation of (1*R*,2*R*)-1,2-diphenylethylenediamine and phenylsalicylate, was synthesized as follows. (1*R*,2*R*)-1,2-diphenylethylenediamine (2.55 g, 12 mmol) and phenylsalicylate (2.57g, 12 mmol) were mixed in a mortar and the solid mixture was ground to be a paste by pestle. The paste material was allowed to stand for 9 h at 80 °C in a dry oven. The resulting yellow solid was dissolved in 30 mL of dichloromethane and the yellow solution was separated by silica gel column chromatography, using Wakogel® C-200) column with 10 cm height and 3 cm diameter. The by-product was removed by eluting 300 mL of dichloromethane, and the desired product was obtained by eluting 120 mL of ethyl acetate. The yellow solution was collected and evaporated to a pale yellow solid. Yield: 2.67 g (67%). As this intermediate compound is unstable, the next reaction was subsequently performed. ^{1}H NMR (600 MHz, $CDCl_3$, 298 K): δ = 12.1 (OH, br s, 1H), 8.00 (ArH, d, *J* = 7.1 Hz, 1H), 7.57 (ArH, dd, *J* = 1.6 and 8.2 Hz 1H), 7.45-7.44 (ArH, m, 2H), 7.41-7.26 (ArH, OH, m, 10H), 6.94-6.90 (ArH, m, 2H), 5.22 ($\underline{\mathrm{CH}}$-NH, dd, *J* = 2.8 and 7.1 Hz, 1H), 4.52 (CH-N, d, *J* = 2.8 Hz, 1H), 1.56 (NH_2, br s, 2H) ppm.

$H_3L^{dpen(1R2R)}$, *N*-((1*R*,2*R*)-2-(((*E*)-3-ethoxy-2-hydroxybenzylidene)amino)-1,2-diphenyl-ethyl)-2-hydroxybenzamide. At the second step, the intermediate compound *N*-((1*R*, 2*R*)-2-amino-1,2-diphenylethyl)-2-hydroxybenzamide was reacted to 3-ethoxysalicyl- aldehyde to give the objective ligand. The intermediate compound (2.67 g, 8.0 mmol) and 3-ethoxysalicylaldehyde (1.33 g, 8.0 mmol) were mixed in 50 mL of methanol and the resulting mixture was warmed on a hot plate for 2 h under stirring. The resulting solution was evaporated to oily material. To the oily material, 30 mL of diethyl ether was added and the solution was stirred for 15 min. Yellow crystalline materials precipitated were collected by suction filtration. Yield: 1.54 g (40%). Anal. Calcd for $H_3L^{dpen(1R2R)}$ = $C_{30}H_{28}N_2O_4$: C, 74.98; H, 5.87; N, 5.83 %. Found: C, 74.85; H, 5.93; N, 5.83 %. ^{1}H NMR (500 MHz, $CDCl_3$, 298 K): δ = 11.8 (OH, s, 1H), 8.05 (CH=N, s, 1H), 7.44-7.13 (ArH, OH, NH, m, 14H), 6.98 (ArH, dd, *J* = 1.1 and 8.0 Hz, 1H), 6.94-6.88 (ArH, m, 2H), 6.81 (dd, *J* = 8.0 and 8.0 Hz, 1H), 6.73 (ArH, dd, *J* = 1.1 and 7.7 Hz, 1H), 5.71 ($\underline{\mathrm{CH}}$-NH, dd, *J* = 2.9 and 8.0 Hz, 1H), 4.85 (CH-N, d, *J* = 3.4 Hz, 1H), 4.16 ($CH_3\underline{CH_2}$, q, *J* = 6.9 Hz, 2H), 1.55 ($\underline{CH_3}CH_2$, t, *J* = 6.9 Hz, 3H) ppm. IR (ATR method, cm^{-1}): ν(C=N) 1626, ν(C=O) 1595.

$H_3L^{dpen(1S2S)}$, *N*-((1*S*,2*S*)-2-(((*E*)-3-ethoxy-2-hydroxybenzylidene)amino)-1,2-diphenylethyl)-2-hydroxybenzamide. The chiral ligand $H_3L^{dpen(1S2S)}$ was prepared by the same method adopted for $H_3L^{dpen(1R2R)}$, using (1*S*,2*S*)-1,2-diphenylethylenediamine instead of (1*R*,2*R*)-1,2-diphenyl- ethylenediamine. Yield: 1.85 g (32%) on the basis of 12 mmol of (1*S*,2*S*)-1,2-diphenyl- ethylenediamine and phenylsalicylate. Anal. Calcd for $H_3L^{dpen(1R2R)}$ = $C_{30}H_{28}N_2O_4$: C, 74.98; H, 5.87; N, 5.83 %. Found: C, 74.93; H, 5.89; N, 5.73 %. ^{1}H NMR (500 MHz, $CDCl_3$, 298 K): δ = 11.8 (OH, s, 1H), 8.05 (CH=N, s, 1H), 7.45-7.19 (ArH, OH, NH, m, 14H), 6.97 (ArH, dd, *J* = 1.1 and 8.0 Hz, 1H), 6.93-6.88 (m, 2H), 6.80 (dd, *J* = 8.0 and 8.0 Hz, 1H), 6.72 (ArH, dd, *J* = 1.1 and 8.0 Hz, 1H), 5.71 ($\underline{\mathrm{CH}}$-NH, dd, *J* = 2.9 and 8.0 Hz, 1H), 4.86 (CH-N, d, *J* = 3.4 Hz, 1H), 4.16 ($CH_3\underline{CH_2}$, q, *J* = 6.9 Hz, 2H), 1.55 ($\underline{CH_3}CH_2$, *J* = 6.9 Hz, 3H) ppm. IR (ATR method, cm^{-1}): ν(C=N) 1626, ν(C=O) 1595.

$Na[Cu^{II}L^{dpen(1R2R/1S2S)}]\cdot H_2O\cdot 0.5CH_3CN$. A solution of copper(II) acetate monohydrate (0.042 g, 0.21 mmol) in 10 mL of methanol was added to a solution of $H_3L^{dpen(1R2R/1S2S)}$ (0.100 g, 0.21 mmol) in 10 mL of methanol. The mixed solution was warmed on a hot plate under stirring for 30 min and then solid of NaOH (0.025g 0.63 mmol) was added and the resulting solution was stirred for 1 h at room temperature. The solution was evaporated to dryness to give a pale brown material. This material was suspended in 100 mL of CH_3CN and small amount of ethanol, and stirred for 30 min on a hot plate. The suspension was then filtered. Red block crystals precipitated from the filtrate during the slow evaporation process and they were collected by suction filtration. Yield: 0.044 g (35%). Anal. Calcd for $Na[Cu^{II}L^{dpen(1R2R/1S2S)}]\cdot H_2O\cdot 0.5CH_3CN$ = $C_{30}H_{25}N_2O_4CuNa\cdot H_2O\cdot 0.5CH_3CN$: C, 61.79; H, 4.77; N, 5.81 %. Found: C, 61.72; H, 4.78; N, 5.76 %. IR (ATR method, cm^{-1}): ν(C=N) 1624, ν(C=O) 1561. TGA: 6.6% weight loss corresponding to $H_2O\cdot 0.5CH_3CN$ molecules (6.4%) was observed in the temperature region lower than 120 °C on the heating process.

$Na[Cu^{II}L^{dpen(1R2R)}]\cdot H_2O$. A solution of copper(II) acetate monohydrate (0.042 g, 0.21 mmol) in 10 mL of methanol was added to a solution of $H_3L^{dpen(1R2R/1S2S)}$ (0.100 g, 0.21 mmol) in 10 mL of methanol. The mixed solution was warmed on a hot plate under stirring for 30 min and then solid of NaOH (0.025g 0.63 mmol) was added and the resulting solution was stirred for 1 h at room temperature. The solution was evaporated to dryness to give a pale brown material. This material was suspended in 100 mL of CH_3CN and small amount of ethanol, and stirred for 30 min on a hot plate. The suspension was then filtered. Red block crystals precipitated from the filtrate during the slow evaporation process and they were collected by suction filtration. Yield: 0.055 g (45%). Anal. Calcd for $Na[Cu^{II}L^{dpen(1R2R)}]\cdot H_2O$ = $C_{30}H_{25}N_2O_4CuNa\cdot H_2O$: C, 61.90; H, 4.68; N, 4.81 %. Found: C, 61.78; H, 4.72; N, 4.89 %. IR (ATR method, cm^{-1}): ν(C=N) 1625, ν(C=O) 1567. TGA: 3.1% weight loss corresponding to H_2O molecule (3.1%) was observed in the temperature region lower than 120 °C on the heating process.

$[Cu^{II}L^{dpen(1R2R/1S2S)}Gd^{III}(NO_3)_2]_2\cdot 0.5CH_3CN$ (1Gd). A solution of $Na[Cu^{II}L^{dpen(1R2R/1S2S)}]\cdot H_2O\cdot 0.5CH_3CN$ (0.060 g, 0.10 mmol) in 30 mL of acetonitrile was added to a solution of $Gd(NO_3)_3\cdot 6H_2O$ (0.045 g, 0.10 mmol) in 10 mL of acetonitrile. The mixture was warmed on a hot plate with stirring for 15 min and filtered. The filtrate was allowed to stand for several days, during which time dark gray crystals precipitated. Yield: 0.021 g (25%). Anal. Calcd. for $(C_{30}H_{25}N_4O_{10}CuGd)_2\cdot 0.5CH_3CN$: C, 44.00; H, 3.12; N 7.15%. Found: C, 44.03; H, 3.31; N 7.12%. IR (ATR method, cm^{-1}): ν(C=N) 1634, ν(C=O) 1574. TGA: 1.4% weight loss corresponding to $0.5CH_3CN$ molecules (1.2%) per tetramer was observed in the temperature region lower than 120 °C on the heating process.

$[Cu^{II}L^{dpen(1R2R/1S2S)}Tb^{III}(NO_3)_2]_2\cdot 2H_2O\cdot 2.5CH_3CN$ (1Tb). The compound was prepared by the same method adopted for $[Cu^{II}L^{dpen(1R2R/1S2S)}Gd^{III}(NO_3)_2]_2$, using $Tb(NO_3)_3\cdot 6H_2O$ instead of $Gd(NO_3)_3\cdot 6H_2O$. Deep green rectangular crystals. Yield: 0.035 g (39%). Anal. Calcd. for $(C_{30}H_{25}N_4O_{10}CuTb)_2\cdot 2H_2O\cdot 2.5CH_3CN$: C, 43.70; H, 3.47; N 8.23%. Found: C, 44.08; H, 3.56; N 8.21%. IR (ATR method, cm^{-1}): ν(C=N) 1634, ν(C=O) 1575. TGA: 7.6% weight loss corresponding to $2H_2O\cdot 2.5CH_3CN$ molecules (7.8%) per tetramer was observed in the temperature region lower than 120 °C on the heating process.

$[Cu^{II}L^{dpen(1R2R/1S2S)}Dy^{III}(NO_3)_2]_2\cdot 2H_2O\cdot 2CH_3CN$ (1Dy). The compound was prepared by the same method adopted for $[Cu^{II}L^{dpen(1R2R/1R2R)}Gd^{III}(NO_3)_2]_2$, using $Dy(NO_3)_3\cdot 6H_2O$ instead of $Gd(NO_3)_3\cdot 6H_2O$. Deep green rectangular crystals. Yield: 0.036 g (41%). Anal. Calcd. for $(C_{30}H_{25}N_4O_{10}CuDy)\cdot 2H_2O\cdot 2CH_3CN$: C, 43.35; H, 3.41; N 7.90%. Found: C, 43.46; H, 3.67; N 7.99%. IR (ATR method, cm^{-1}): ν(C=N) 1634, ν(C=O) 1576. TGA: 7.1% weight loss corresponding to $2H_2O\cdot 2CH_3CN$ molecules (6.7%) per tetramer was observed in the temperature region lower than 120 °C on the heating process.

$[Cu^{II}L^{dpen(1R2R)}Gd^{III}(NO_3)_2]_{1\infty}\cdot 1.5H_2O$ (2Gd). A solution of $Na[CuL^{dpen(1R2R)}]\cdot H_2O$ (0.058 g, 0.10 mmol) in 30 mL of acetonitrile was added to a solution of $Gd(NO_3)_3\cdot 6H_2O$ (0.045 g, 0.10 mmol) in 10 mL of acetonitrile. The mixture was warmed on a hot plate with stirring for 30 min and filtered. The filtrate was allowed to stand for several days, during which time square block red crystals precipitated. Yield: 0.028 g (33%). Anal. Calcd. for $C_{30}H_{25}N_4O_{10}CuGd\cdot 1.5H_2O$: C, 42.42; H, 3.32; N 6.60%. Found: C, 42.60; H, 3.51; N 6.61%. IR (ATR method, cm^{-1}): ν(C=N) 1633, ν(C=O) 1570. TGA: 3.4% weight loss corresponding to $1.5H_2O$ molecules (3.2%) per dimer was observed in the temperature region lower than 120 °C on the heating process.

$[Cu^{II}L^{dpen(1R2R)}Tb^{III}(NO_3)_2]_{1\infty}\cdot 1.5H_2O$ (2Tb). The compound was prepared by the same method adopted for $[Cu^{II}L^{dpen(1R2R)}Gd^{III}(NO_3)_2]_{1\infty}$, using $Tb(NO_3)_3\cdot 6H_2O$ instead of $Gd(NO_3)_3\cdot 6H_2O$. Red crystals. Yield: 0.030 g (35%). Anal. Calcd. for $C_{30}H_{25}N_4O_{10}CuTb\cdot 1.5H_2O$: C, 42.34; H, 3.32; N 6.58%. Found: C, 42.17; H, 3.38; N 6.64%. IR (ATR method, cm^{-1}): ν(C=N) 1634, ν(C=O) 1570. TGA: 3.3% weight loss corresponding to $1.5H_2O$ molecules (3.2%) per dimer was observed in the temperature region lower than 120 °C on the heating process.

$[Cu^{II}L^{dpen(1R2R)}Dy^{III}(NO_3)_2]_{1\infty}\cdot 1.5H_2O$ (2Dy). The compound was prepared by the same method adopted for $[Cu^{II}L^{dpen(1R2R)}Gd^{III}(NO_3)_2]_{1\infty}$, using $Dy(NO_3)_3\cdot 6H_2O$ instead of $Gd(NO_3)_3\cdot 6H_2O$. Red crystals. Yield: 0.031 g (36%). Anal. Calcd. for $C_{30}H_{25}N_4O_{10}CuDy\cdot 1.5H_2O$: C, 42.16; H, 3.30; N 6.56%. Found: C, 42.06; H, 3.43; N 6.60%. IR (ATR method, cm^{-1}): ν(C=N) 1634, ν(C=O) 1570. TGA: 3.8% weight loss corresponding to $1.5H_2O$ molecules (3.2%) per dimer was observed in the temperature region lower than 120 °C on the heating process.

Physical Measurements. Elemental C, H, and N analyses were carried out at the Center for Instrumental Analysis of Kumamoto University. Infrared spectra were recorded at room temperature using a PerkinElmer Frontier MIR/NIR spectrometer with attenuated total reflectance (ATR) method. Thermogravimetric analyses (TGA) were performed on a TG/DTA6200 (Seiko Instrument Inc.). The samples of ca. 3 mg were heated from room temperature to 120 ºC in the heating mode at the heating rate of 10 ºC min^{-1}, kept the temperature for 30 min, and then cooled to room temperature. ^1H NMR was recorded at 600 MHz on a JEOL 600-ECA instrument. Fast-atom-bombardment mass spectrometry spectra were measured in methanol or DMSO on a JEOL JMS-700 mass spectrometer; 3-nitrobenzylalcohol was used as the matrix.

Temperature-dependent magnetic susceptibilities in the temperature range 1.9–300 K at an external magnetic field of 0.1 T and field-dependent magnetization measurements in an applied magnetic field from 0 to 5 T at 1.9 K were measured with an MPMS XL5 SQUID susceptometer (Quantum Design, Inc.). For the temperature dependent-magnetic susceptibility measurements, samples were fixed with a small amount of liquid paraffin to avoid orientation in the field. For the magnetization measurements, samples with and without liquid paraffin were measured. The calibrations were performed with palladium. Corrections for diamagnetism were applied using Pascal's constants.[13] Ac magnetic susceptibility was measured on a PPMS ac/dc magnetometer (Quantum Design, Inc.) in a temperature range down to 1.9 K at 0 and 1000 Oe dc fields.

X-ray Crystal Structure Analysis. The single-crystal X-ray diffraction data were collected by a Rigaku RAXIS RAPID imaging plate diffractometer using graphite-monochromated Mo Kα radiation at 120 K for **2Gd**, **2Tb**, **2Dy** and 150 K for the other complexes. All the crystals were quickly picked up from the mother liquid, coated by epoxy resin, and used for the X-ray diffraction study at the settled low temperature. The temperature of the crystal was maintained within an accuracy of ± 2 K by a Rigaku N_2 cryostat. The structures were solved by direct methods and expanded using the Fourier technique.[28] Hydrogen atoms were positioned at the calculated positions and refined using a riding model. All calculations were performed using the CrystalStructure crystallographic software package.[29]

Table 3. X-ray Crystallographic Data for $[\mathrm{Cu^{II}L^{dpen(1R2R/1S2S)}Gd^{III}(NO_3)_2}]$ (1Gd), $[\mathrm{Cu^{II}L^{dpen(1R2R/1S2S)}(H_2O)Tb^{III}(NO_3)_2}]\cdot\mathrm{CH_3CN}$ (1Tb), $[\mathrm{Cu^{II}L^{dpen(1R2R/1S2S)}(CH_3CN)Dy^{III}(NO_3)_2}]$ (1Dy), $[\mathrm{Cu^{II}L^{dpen(1R2R)}Gd^{III}(NO_3)_2(CH_3CN)}]_{1\infty}\cdot\mathrm{CH_3CN}$ (2Gd), $[\mathrm{Cu^{II}L^{dpen(1R2R)}Tb^{III}(NO_3)_2(CH_3CN)}]_{1\infty}\cdot\mathrm{CH_3CN}$ (2Tb), and $\mathrm{Cu^{II}L^{dpen(1R2R)}Dy^{III}(NO_3)_2(CH_3CN)}]_{1\infty}\cdot\mathrm{CH_3CN}$ (2Dy)

	1Gd	**1Tb**	**1Dy**	**2Gd**	**2Tb**	**2Dy**
formula	$C_{30}H_{25}N_4O_{10}CuGd$	$C_{32}H_{30}N_5O_{11}CuTb$	$C_{32}H_{28}N_5O_{10}CuDy$	$C_{34}H_{31}N_6O_{10}CuGd$	$C_{34}H_{31}N_6O_{10}CuTb$	$C_{34}H_{31}N_6O_{10}CuDy$
fw	822.34	883.09	868.65	904.45	906.12	909.70
cryst syst	triclinic	monoclinic	monoclinic	orthorhombic	orthorhombic	orthorhombic
space group	P-1 (No.2)	$P2_1/n$ (No.14)	$P2_1/n$ (No.14)	$P2_12_12_1$ (No.19)	$P2_12_12_1$ (No.19)	$P2_12_12_1$ (No.19)
a, Å	9.1079(5)	12.9359(4)	13.1609(4)	13.4892(4)	13.478(4)	13.5310(4)
b, Å	12.6756(7)	14.6473(4)	16.3506(4)	15.7803(4)	15.682(5)	15.7064(4)
c, Å	13.7264(8)	18.4054(7)	16.2739(5)	15.8966(5)	15.861(4)	15.8985(4)
α, deg.	81.687(2)	-	-	-	-	-
β, deg.	83.994(2)	110.823(1)	106.640(1)	-	-	-
γ, deg.	71.646(2)	-	-	-	-	-
V, Å^3	1485.3(2)	3259.6(2)	3355.3(2)	3383.8(2)	3352.4(17)	3378.8(2)
Z	2	4	4	4	4	4
T, K	150	150	150	120	120	120
$F(000)$	812.00	1756.00	1720.00	1800.00	1804.00	1808.00
$D_{\mathrm{calcd.}}$, g cm^{-3}	1.839	1.799	1.719	1.775	1.795	1.788
μ, mm^{-1}	3.0011	2.8697	2.9108	2.6453	2.7915	2.8958
λ, Å	0.71075	0.71075	0.71075	0.71075	0.71075	0.71075
R, Rw	0.0485, 0.0962	0.0222, 0.0248	0.0337, 0.0389	0.0418, 0.0809	0.0188, 0.0676	0.0414, 0.0813
Flack parameter	-	-	-	0.025(15)	−0.015(3)	−0.006(16)

Table 4. Selected Coordination Bond Lengths (Å) and Angles (°) for $[\mathrm{Cu^{II}L^{dpen(1R2R/1S2S)}Gd^{III}(NO_3)_2}]$ (1Gd), $[\mathrm{Cu^{II}L^{dpen(1R2R/1S2S)}(H_2O)Tb^{III}(NO_3)_2}]\cdot\mathrm{CH_3CN}$ (1Tb), $[\mathrm{Cu^{II}L^{dpen(1R2R/1S2S)}(CH_3CN)Dy^{III}(NO_3)_2}]$ (1Dy), $[\mathrm{Cu^{II}L^{dpen(1R2R)}Gd^{III}(NO_3)_2(CH_3CN)}]_{1\infty}\cdot\mathrm{CH_3CN}$ (2Gd), $[\mathrm{Cu^{II}L^{dpen(1R2R)}Tb^{III}(NO_3)_2(CH_3CN)}]_{1\infty}\cdot\mathrm{CH_3CN}$ (2Tb), and $[\mathrm{Cu^{II}L^{dpen(1R2R)}Dy^{III}(NO_3)_2(CH_3CN)}]_{1\infty}\cdot\mathrm{CH_3CN}$ (2Dy)

	1Gd	**1Tb**	**1Dy**	**2Gd**	**2Tb**	**2Dy**
Bond Lengths (Å)						
Ln1−Cu1	3.370(1)	3.3569(3)	3.3511(4)	3.3348(9)	3.3112(9)	3.3094(11)
Ln1−Cu1*	5.627(1)	5.7174(3)	5.5443(4)	6.2326(9)	6.200(2)	6.211(1)
Ln1−O1	2.353(5)	2.3445(11)	2.3185(18)	2.440(5)	2.426(4)	2.411(5)
Ln1−O2	2.311(5)	2.2680(14)	2.2696(19)	2.315(5)	2.298(4)	2.291(6)
Ln1−O3*	2.267(7)	2.2249(13)	2.220(2)	2.228(5)	2.216(4)	2.206(6)
Ln1−O4	2.502(5)	2.4754(12)	2.4719(19)	2.675(5)	2.665(3)	2.657(6)
Ln1−O5	2.466(8)	2.4402(13)	2.396(3)	2.534(5)	2.534(4)	2.526(6)
Ln1−O6	2.460(7)	2.4889(16)	2.403(4)	2.415(5)	2.403(4)	2.405(6)
Ln1−O8	2.444(6)	2.4454(14)	2.459(3)	2.437(6)	2.427(4)	2.409(7)
Ln1−O9	2.405(6)	2.4177(17)	2.395(3)	2.485(5)	2.484(4)	2.477(6)
Ln1−N5	-	-	-	2.570(7)	2.561(5)	2.546(8)
Cu1−O1	1.920(5)	1.9386(13)	1.9488(18)	1.914(5)	1.904(3)	1.911(5)
Cu1−O2	1.935(5)	1.9393(12)	1.9363(19)	1.924(5)	1.916(4)	1.913(6)
Cu1−O11	-	2.4146(16)	-	-	-	-
Cu1−N5	-	-	2.413(3)	-	-	-
Cu1−N1	1.911(6)	1.9242(14)	1.919(3)	1.899(6)	1.889(4)	1.878(7)
Cu1−N2	1.926(6)	1.9413(16)	1.947(2)	1.925(6)	1.922(4)	1.927(7)
Bond Angles (°)						
O1−Ln1−O2	67.36(16)	68.08(5)	68.25(7)	65.08(15)	65.35(12)	65.39(19)
O1−Ln1−O3*	78.8(2)	79.81(5)	83.34(8)	142.3(2)	142.34(12)	142.33(18)
O2−Ln1−O3*	100.3(2)	94.86(5)	94.90(7)	98.7(2)	98.93(13)	99.0(2)
O3*−Ln1−O4	92.4(2)	86.40(4)	82.53(8)	75.8(2)	76.15(12)	76.1(2)
O3*−Ln1−O5	146.80(19)	152.89(5)	149.63(8)	73.3(2)	73.30(12)	72.98(19)
O3*−Ln1−O6	159.4(2)	156.06(5)	155.63(9)	85.6(2)	84.59(13)	84.6(2)
O3*−Ln1−O8	94.4(3)	92.86(5)	83.21(8)	107.8(2)	106.91(13)	107.4(2)
O3*−Ln1−O9	84.7(2)	93.66(6)	91.51(9)	77.1(2)	76.81(13)	76.81(19)
O1−Cu1−O2	84.3(2)	83.52(6)	83.00(8)	83.7(2)	83.86(15)	83.3(3)
O1−Cu1−O11	-	89.89(6)	-	-	-	-
O1−Cu1−N5	-	-	90.59(9)	-	-	-
O1−Cu1−N1	97.3(3)	96.62(6)	96.78(9)	98.0(2)	98.07(17)	98.8(3)
O1−Cu1−N2	176.7(3)	173.68(6)	170.92(9)	175.8(2)	175.79(17)	175.7(3)
O2−Cu1−O11	-	93.85(6)	-	-	-	-
O2−Cu1−N5	-	-	92.99(9)	-	-	-
O2−Cu1−N1	175.0(3)	164.97(6)	165.87(10)	177.8(3)	177.38(17)	177.4(3)
O2−Cu1−N2	92.5(3)	92.56(6)	92.30(8)	92.4(3)	92.30(17)	92.7(3)
N1−Cu1−N2	86.0(3)	85.87(6)	85.87(9)	85.8(3)	85.71(18)	85.2(3)
Ln1−O1−Cu1	103.66(19)	102.80(5)	103.15(8)	99.26(18)	99.03(14)	99.3(2)
Ln1−O2−Cu1	104.71(19)	105.59(6)	105.37(8)	103.4(2)	103.20(15)	103.5(3)
Ln1−O3*−C7*	133.9(5)	138.82(12)	132.22(18)	177.6(4)	177.0(3)	177.1(6)

1Gd (*^{1}; 1−x, 1−y, 1−z), **1Tb** and **1Dy** (*^{2}; 1−x, 1−y, −z), and **2Ln** (*^{3}; 1−x, −1/2+y, 1/2−z)

ASSOCIATED CONTENT

* Supporting Information

X-ray crystallographic files (CIF) are available free of charge via the Internet at http://pubs.acs.org. X-ray crystallographic data in CIF format for Na[Cu^{II}L$^{dpen(1R2R/1S2S)}$] and Na[Cu^{II}L$^{dpen(1R2R)}$] (CCDC 1485912, 1485904), **1Gd**, **1Tb**, **1Dy** (CCDC 1485913, 1401600, 1485914) and **2Gd**, **2Tb**, **2Dy** (CCDC 1485915, 1401601, 1485916) can be obtained via http://www.ccdc.cam.ac.uk/conts/retrieving.html or from the Cambridge Crystallographic Data Centre, 12 Union Road, Cambridge CB2 1EZ, U.K. [fax (+44)1223−336−033; e-mail deposit@ccdc.cam.ac.uk].

AUTHOR INFORMATION

Corresponding Author

*E-mail: naohide@aster.sci.kumamoto-u.ac.jp. Fax: +81-96-342-3390.

*E-mail: sunatuki@cc.okayama-u.ac.jp. Fax: +81-86-251-7833.

Notes

The authors declare no competing financial interest.

ACKNOWLEDGMENTS

T. Fujinami and T. Kanetomo were supported by the JSPS program for Research Fellowships for Young Scientist (No. 20360300 and No. 15J11497). This work was supported by JSPS KAKENHI Grant-in-Aid for Scientific Research(C) #15K05455 (Y. Sunatsuki).

REFERENCES

(1) (a) Lehn, J.-M. Supramolecular Chemistry: Concepts and Perspectives; VCH: Weinheim, 1995. (b) Leininger, S.; Olenyuk, B.; Stang, P. J. *Chem. Rev.* **2000**, *100*, 853−908. (c) Caulder, D. L.; Raymond, K. N. *Acc. Chem. Res.* **1999**, *32*, 975−982. (d) Fujita, M.; Tominaga, M.; Hori, A.; Therrien, B. *Acc. Chem. Res.* **2005**, *38*, 371−380. (e) Fujita, M.; Uemoto, K.; Yoshizawa, M.; Fujita, N.; Kusukawa, T.; Biradha, K. *Chem. Commun*. **2001**, 509–518.

(2) (a) Pei, Y.; Verdaguer, M.; Kahn, O.; Sletten, J.; Renard, J. P. *Inorg. Chem.* **1987**, *26*, 138−143. (b) Kahn, O.; Pei, Y.; Verdaguer, M.; Renard, J. P.; Sletten, J. *J. Am. Chem. Soc*. **1988**, *110*, 782–789.

(3) (a) Caneschi, A.; Gatteschi, D.; Rey, P.; Sessoli, R. *Inorg. Chem.* **1988**, *27*, 1756−1761. (b) Caneschi, A.; Gatteschi, D.; Laugier, J.; Rey, P.; Sessoli, R.; Zanchini, J. *J. Am. Chem. Soc*. **1988**, *110*, 2795−2799.

(4) (a) Miller, J. S.; Calabrese, J. C.; Rommelmann, H.; Chittipeddi, S. R.; Zhang, J. H.; Reiff, W. M.; Epstein, A. J. *J. Am. Chem. Soc*. **1987**, *109*, 769–871. (b) Miller, J. S.; Epstein, A. J. *J. Am. Chem. Soc.* **1987**, *109*, 3850–3855. (c) Miller, J. S.; Epstein, A. J. *Angew. Chem. Int. Engl.* **1994**, *33*, 385–415.

(5) Tamaki, H.; Zhong, Z. J.; Matsumoto, N.; Kida, S.; Koikawa, M.; Achiwa, N.; Hashimoto, Y.; Okawa, H. *J. Am. Chem. Soc.* **1992**, *114*, 6974–6979.

(6) (a) Miyasaka, H.; Matsumoto, N.; Ohkawa, H.; Re, N.; Gallo, E.; Floriani, C. *J. Am. Chem. Soc.* **1996**, *118*, 981–994. (b) Re, N.; Gallo, E.; Floriani, C.; Miyasaka, H.; Matsumoto, N. *Inorg. Chem.* **1996**, *35*, 6004–6008.

(7) (a) Ohba, M.; Okawa, H.; *Coord. Chem. Revs.* **2000**, *198*, 313–328. (b) Ohba, M.; Maruono, N.; Okawa, H.; Enoki, T.; Latour, J. M. *J. Am. Chem. Soc.* **1994**, *116*, 11566–11567.

(8) Matsumoto, N.; Motoda, Y.; Matsuo, T.; Nakashima, T.; Re, N.; Dahan, F.; Tuchagues, J. P. *Inorg. Chem.* **1999**, *38*, 1165–1173.

(9) (a) Collet, A.; Brienne, M. J.; Jacques, J. *Chem. Rev.* **1980**, *80*, 215-250. (b) Kuroda, R.; Mason, S. F. *J. Chem. Soc. Dalton. Trans.* **1981**, 1268-1273. (c) Katsuki, I.; Motoda, Y.; Sunatsuki, Y.; Matsumoto, N.; Nakashima, T.; Kojima, M. *J. Am. Chem. Soc.* **2002**, *124*, 629–640. (d) Sato, T.; Nishi, K.; Iijima, S.; Kojima, M.; Matsumoto, N. *Inorg. Chem.* **2009**, *48*, 7211–7229.

(10) (a) Hoshino, N.; Sekine, Y.; Nihei, M.; Oshio, H. *Chem. Commun.* **2010**, *46*, 6117–6119. (b) Oishi, T.; Hashibe, T.; Takahashi, S.; Hagiwara, H.; Matsumoto, N.; Sunatsuki, Y. *Polyhedron*, **2012**, *33*, 209–217. (c) Hamamatsu, T.; Matsumoto, N.; Re, N.; Mrozinski, J. *Chem. Lett.* **2009**, *38*, 762–763. (d) Shimogori, Y.; Hamamatsu, T.; Fujinami, T.; Hagiwara, H.; Matsumoto, N.; Re, N.; Mrozinski, J.; Ishikawa, Y.; Igashira-Kamiyama, A.; Konno, T. *Polyhedron* **2011**, *30*, 1127–1133.

(11) (a) Amori, H.; Gruselle, M. *Chirality in Transition Metal Chemistry: Molecules, Supramolecular Assemblies and Materials*, John Wiley & Sons, Chichester, **2008**. (b) Train, C.; Gruselle, M.; Verdaguer, M. *Chem. Soc. Rev.* **2011**, *12*, 3297−3312. (c) Rikken, G. L. J. A.; Raupach, E. *Nature*, **2000**, *405*, 932–935.

(12) (a) Cimpoesu, F.; Dahan, F.; Ladeira, S.; Ferbinteanu, M.; Costes, J. P. *Inorg. Chem.* **2012**, *51*, 11279−11293. (b) Margeat, O.; Lacroix, P. G.; Costes, J. P.; Donnadieu, B.; Lepetit, C. *Inorg. Chem.* **2004**, *43*, 4743−4750. (c) Sui, Y.; Liu, D. S.; Hu, R. H.; Huang, J. G. *Inorg. Chim. Acta* **2013**, *395*, 225–229. (d) Li, L.; Nishihara, S.; Inoue, K.; Kurmoo, M. *Inorg. Chem.* **2016**, *55*, 300–306. (e) Mito, M.; Iriguchi, K.; Deguchi, H.; Kishine, J. I.; Kikuchi, K.; Ohsumi, H.; Yoshida, Y.; Inoue, K. *Phys. Rev. B* **2009**, *79*, 012406-1–012406-3. (f) Long, J.; Rouquette, J.; Thibaud, J-M.; Ferreira, R. A.; Carlos, L. D.; Donnadieu, B.; Vieru, V.; Chibotaru, L. F.; Konczewicz, L.; Haines, J.; Guari, Y.; Larionova, J. *Angew. Chem. Int. Ed.* **2015**, *54*, 2236–2240. (g) Train, C.; Nuida, T.; Gheorghe, R.; Gruselle, M.; Ohkoshi, S. *J. Am. Chem. Soc.* **2009**, *131*, 16838–16843.

(13) Kahn, O. *Molecular Magnetism*; VCH: New York, **1993**. Chapter 3.

(14) (a) Towatari, M.; Nishi, K.; Fujinami, T.; Matsumoto, N.; Sunatsuki, Y.; Kojima, M.; Mochida, N.; Ishida, T.; Re, N.; Mrozinski, J. *Inorg. Chem.* **2013**, *52*, 6160−6178. (b) Kido, T.; Ikuta, Y.; Sunatsuki, Y.; Ogawa, Y.; Matsumoto, N.; Re, N. *Inorg. Chem.* **2003**, *42*, 398−408. (c) Costes, J.-P.; Dahan, F.; Dupuis, A.; Laurent, J.-P. *Chem. Eur. J.* **1998**, *4*, 1616−1620.

(15) (a) Sessoli, R.; Gatteschi, D.; Caneschi, A.; Novak, M. A. *Nature* **1993**, *365*, 141–143. (b) Sessoli, R.; Tsai, H. L.; Schake, A. R.; Wang, S.; Vincent, J. B.; Folting, K.; Gatteschi, D.; Christou, G.; Hendrickson, D. N. *J. Am. Chem. Soc.* **1993**, *115*, 1804–1816. (c) Gatteschi, D.; Sessoli, R. *Angew. Chem. Int. Ed.* **2003**, *42*, 268–297.

(16) (a) Gatteschi, D.; Sessoli, R.; Villain, J. *Molecular Nanomagnets*, Oxford University Press, New York, **2006**. (b) Sessoli, R. *Angew. Chem. Int. Ed.* **2008**, *47*, 5508–5510. (c) Bernot, K.; Bogani, L.; Caneschi, A.; Gatteschi, D.; Sessoli, R. *J. Am. Chem. Soc.* **2006**, *128*, 7947–7956.

(17) (a) Ishikawa, N.; Sugita, M.; Ishikawa, T.; Koshihara, S. Y.; Kaizu, Y. *J. Am. Chem. Soc.* **2003**, *125*, 8694−8695. (b) Sessoli, R.; Powell, A. K. *Coord. Chem. Rev.* **2009**, *253*, 2328−2341. (c) Sorace, L.; Benelli, C.; Gatteschi, D. *Chem. Soc. Rev.* **2011**, *40*, 3092−3104. (d) Woodruff, D. N.; Winpenny, R. E. P.; Layfield, R. A. *Chem. Rev.* **2013**, *113*, 5110−5148.

(18) (a) Osa, S.; Kido, T.; Matsumoto, N.; Re, N.; Pochaba, A.; Mronzinski, J. *J. Am. Chem. Soc.* **2004**, *126*, 420–421; (b) Costes, J.-P.; Dahan, F.; Wernsdorfer, W. *Inorg. Chem.* **2006**, *45*, 5–7. (c) Costes, J.-P.; Auchel, M.; Dahan, F.; Peyrou, V.; Shova, S.; Wernsdorfer, W. *Inorg. Chem.* **2006**, *45*, 1924–1934. (c) Kajiwara, T.; Nakano, M.; Takahashi, K.; Takaishi, S.; Yamashita, M. *Chem.-Eur. J.* **2011**, *17*, 196–205. (d) Ferbinteanu, M.; Kajiwara, T.; Choi, K. Y.; Nojiri, H.; Nakamoto, A.; Kojima, N.; Cimpoesu, F.; Fujimura, Y.; Takaishi, S.; Yamashita, M. *J. Am. Chem. Soc.* **2006**, *128*, 9008–9009. (e) Mori, F.; Nyui, T.; Ishida, T.; Nogami, T.; Choi, K.-Y.; Nojiri, H. *J. Am. Chem. Soc.* **2006**, *128*, 1440–1441. (f) S. Ueki, Ishida, T.; Nogami, T.; Choi, K.-Y.; Nojiri, H. *Chem. Phys. Lett.* **2007**, *440*, 263–267. (g) Okazawa, A.; Nogami, T.; Nojiri, H.; Ishida, T. *Chem. Mater.* **2008**, *20*, 3110. (h) Gao, Y.; Zhao, L.; Xu, X.; Xu, G.-F.; Guo, Y.-N.; Tang, J.; Liu, Z. *Inorg. Chem.* **2011**, *50*, 1304–1308. (i) Colacio, E.; Ruiz, J.; Mota, A. J.; Palacios, M. A.; Cremades, E.; Ruiz, E.; White, F. J.; Euan K. Brechin, E. K. *Inorg. Chem.* **2012**, *51*, 5857–5868. (j) Efthymiou, C. G.; Stamatatos, T. C.; Papatriantafyllopoulou, C.; Tasiopoulos, A. J.; Wernsdorfer, W.; Perlepes, S. P.; Christou, G. *Inorg. Chem.* **2010**, *49*, 9737–9739. (k) Burrow, C. E.; Burchell, T. J.; Lin, P.-H.; Habib, F.; Wernsdorfer, W.; Clérac, R.; Murugesu, M. *Inorg. Chem.* **2009**, *48*, 8051–8053. (l) Feltham, H. L. C.; Lan, Y.; Klower, F.; Ungur, L.; Chibotaru, L. F.; Powell, A. K.; Brooker, S. *Chem. Eur. J.* **2011**, *17*, 4362–4365.

(19) (a) Caneschi, A.; Gatteschi, D.; Lalioti, N.; Sangregorio, C.; Sessoli, R.; Venturi, G.; Vindigni, A.; Rettori, A.; Pini, M. G.; Novak, M. A. *Angew. Chem. Int. Ed.* **2001**, *40*, 1760–1763. (b) Clérac, R.; Miyasaka, H.; Yamashita, M.; Coulon, C.; *J. Am. Chem. Soc.* **2002**, *124*, 12837–12844; (c) Kajiwara, T.; Watanabe, I.; Kaneko, Y.; Takaishi, S.; Enomoto, M.; Kojima, N.; Yamashita, M.; *J. Am. Chem. Soc.* **2007**, *129*, 12360–12361. (d) Ishii, N.; Okamura, Y.; Chiba, S.; Nogami, T.; Ishida, T.; *J. Am. Chem. Soc.* **2008**, *130*, 24–25. (e) Costes, J. P.; Clemente-Juan, J. M.; Dahan, F.; Milon, J. *Inorg. Chem.* **2004**, *43*, 8200–8202.

(20) Llunell, M.; Casanova, D.; Cirera, J.; Alemany, P.; Alvarez, S. SHAPE, v2.1; University of Barcelona and The Hebrew University of Jerusalem, Barcelona and Jerusalem, 2013.

(21) (a) Isabelle, R.; Olivier, K.; Yves, J.; Francis, R.; *Inorg. Chem.* **1997,** *36*, 930–936. (b) Matsumoto, N.; Kimoto, K.; Ohyoshi, A.; Maeda, Y. *Bull. Chem. Soc. Jpn*. **1984**, *57*, 3307–3311.

(22) Costes, J.P.; Auchel, M.; Dahan, F.; Peyrou, V.; Shova, S.; Wernsdorfer, W. *Inorg. Chem.* **2006**, *45*, 1924–1934, and references therein; (b) Costes, J.P.; Duhayon, C.; Mallet-Ladeira, S.; Shova, S.; Vendier, L. *Chem. Eur. J.* **2016**, *22*, 2171 –2180.

(23) Novitchi, G.; Costes, J.P.; Donnadieu, B. *Eur. J. Inorg. Chem*. **2004**, 1808–1812.

(24) Fisher, M. E. *Am. J. Phys*. **1964**, *32*, 343–346.

(25) Deorges, R.; Borra`s-Almenar, J.; Coronado, E.; Cure´ly, J.; Drillon, M. One-Dimensional Magnetism: An Overview of the Models. In Magnetism: Molecules to Materials (Eds: J. S. Miller, M. Drillon, Wiley-VCH, **2001**.

(26) Cole, K. S.; Cole, H. R. *J. Chem. Phys*. **1941**, *9*, 341–352.

(27) Castro, S. L.; Sun, Z.; Grant, C. M.; Bollinger, J. C.; Hendrickson, D. N.; Christou, G. *J. Am. Chem. Soc.* **1998**, *120*, 2365−2375. Ako, A.; Mereacre, M.; Hewitt, I. J.; Clerac, R.; Lecren, L.; Anson, C. E.; Powell, A. K. *J. Mater. Chem.* **2006**, *16*, 2579−2586. Okazawa, A.; Nojiri, H.; Ishida, T.; Kojima, N. *Polyhedron 2011*, *30*, 3140−3144. Kajiwara, T.; Nakano, M.; Takaishi, S.; Yamashita, M. *Inorg. Chem*. **2008**, *47*, 8604−8606.

(28) (a) SIR92, A. Altomare, G. Cascarano, C. Giacovazzo, A. Guagliardi, M. Burla, G. Polidori, M. Camalli, J. Appl. Cryst. 27 (1994) 435. (b) DIRDIF-99, P. T. Beurskens, G. Admiraal, G. Beurskens, W. P. Bosman, R. de Gelder, R. Israel, J. M. M. Smits, The DIRDIF-99 program system, Technical Report of the Crystallography Laboratory, University of Nijmegen, The Netherlands, 1999.

(29) CrystalStructure 4.0: Crystal Structure Analysis Package, Rigaku Corporation (2000–2010), Tokyo, Japan.

SYNOPSIS TOC (Word Style "SN_Synopsis_TOC"). If you are submitting your paper to a journal that requires a synopsis graphic and/or synopsis paragraph, see the Instructions for Authors on the journal's homepage for a description of what needs to be provided and for the size requirements of the artwork.

To format double-column figures, schemes, charts, and tables, use the following instructions:

Place the insertion point where you want to change the number of columns
From the **Insert** menu, choose **Break**
Under **Sections**, choose **Continuous**
Make sure the insertion point is in the new section. From the **Format** menu, choose **Columns**
In the **Number of Columns** box, type **1**
Choose the **OK** button

Now your page is set up so that figures, schemes, charts, and tables can span two columns. These must appear at the top of the page. Be sure to add another section break after the table and change it back to two columns with a spacing of 0.33 in.

Authors are required to submit a graphic entry for the Table of Contents (TOC) that, in conjunction with the manuscript title, should give the reader a representative idea of one of the following: A key structure, reaction, equation, concept, or theorem, etc., that is discussed in the manuscript. Consult the journal's Instructions for Authors for TOC graphic specifications.

Insert Table of Contents Graphic and Synopsis Here **Graphical abstract**

The assembly reaction of the racemic form of the "cross-linking ligand-complex" Na[$\mathrm{Cu^{II}L^{dpen(1R2R/1S2S)}}$] with $\mathrm{Ln^{III}(NO_3)_3 \cdot 6H_2O}$ gave a centrosymmetric circular $\mathrm{(Cu^{II}Ln^{III})_2}$ complex $\mathrm{[Cu^{II}L^{dpen(1R2R/1S2S)}Ln^{III}(NO_3)_2]_2}$ (**1Gd**, **1Tb**, **1Dy**), while the reaction using the enantiopure form gave a chiral chainlike $\mathrm{(Cu^{II}Ln^{III})_{1\infty}}$ complex $\mathrm{[Cu^{II}L^{dpen(1R2R)}Ln^{III}(NO_3)_2(CH_3CN)]_{1\infty} \cdot CH_3CN}$ (**2Gd**, **2Tb**, **2Dy**). The bridged angles through the amido group of Gd−O3*=C7* are 133.9(5)° and 177.6(4)° for **1Gd** and **2Gd**, respectively. The $\mathrm{Cu^{II}}$-$\mathrm{Gd^{III}}$ magnetic interaction through two phenoxo bridges (J_1) and a three-atom N−C=O bridge (J_2) are both positive and the magnitude of the J_2 value of **2Gd** is much smaller than that of **1Gd**. **1Ln** and **2Ln** showed strong magnetic anisotropy. **1Tb** and **1Dy** showed frequency dependence of AC magnetic susceptibility under zero external DC magnetic field, indicating the behavior of single-molecule magnets (SMMs). **2Tb** and **2Dy** showed no frequency dependence under zero external magnetic field, but showed a meaningful frequency dependence under an external magnetic field.